TU Delft

Delft University of Technology

Document Version
Final published version

Licence
CC BY

Citation (APA)
van den Berg, M., Labeur, R. J., Aarninkhof, S. G. J., & Visser, P. J. (2025). Exploring the effect of foreshores on dike breach development via a mid-scale experiment. *Journal of Coastal and Hydraulic Structures*, *5*, Article 43. https://doi.org/10.59490/jchs.2025.0043

Important note
To cite this publication, please use the final published version (if applicable).
Please check the document version above.

Copyright
In case the licence states “Dutch Copyright Act (Article 25fa)”, this publication was made available Green Open Access via the TU Delft Institutional Repository pursuant to Dutch Copyright Act (Article 25fa, the Taverne amendment). This provision does not affect copyright ownership.
Unless copyright is transferred by contract or statute, it remains with the copyright holder.

Sharing and reuse
Other than for strictly personal use, it is not permitted to download, forward or distribute the text or part of it, without the consent of the author(s) and/or copyright holder(s), unless the work is under an open content license such as Creative Commons.

Takedown policy
Please contact us and provide details if you believe this document breaches copyrights.
We will remove access to the work immediately and investigate your claim.

This work is downloaded from Delft University of Technology.

JOURNAL OF COASTAL AND HYDRAULIC STRUCTURES

Vol. 5, 2025, 43

Exploring the effect of foreshores on dike breach development via a mid-scale experiment

Mario van den Berg[1], Robert J. Labeur[2], Stefan G.J. Aarninkhof[3], and Paul J. Visser[4]

Abstract

Coastal and fluvial flood defences currently rely primarily on existing (grey) infrastructure such as dikes. However, coastal flood risk is expected to increase substantially in the near future. This requires ever increasing efforts to strengthen dikes. To aid these conventional methods, Nature-based Solutions (NbS) are increasingly proposed, such as coastal wetlands. Coastal wetlands have many ecological benefits, but also aid flood protection, especially tidal marshes. Tidal marshes protect the dikes behind them through wave attenuation and reduce flood damage if the dike is breached. Meanwhile, flood risk assessment relies on dike breach modelling to estimate the breach discharges for inundation simulations. Yet, how these foreshores (e.g., tidal marsh) affect dike breach development is largely unknown. For this reason, we experimentally explore how different foreshores affect the dike breaching process. In this study we performed a series of breach tests with a 1.5-1.9 m high model sand-dike with and without a foreshore. Two types of foreshores were tested, an erodible sand as a proxy for a beach/sandy wetland and a low-erodible clay layer as a proxy for an unvegetated tidal marsh. Because dike breach flow closely resembles weir flow, the standard weir equation applies, which is also frequently used in breach discharge models. The observed foreshore effects are qualitatively evaluated using this weir equation. Depending on foreshore stability, we find that foreshores affect breach hydrodynamics which alters the weir shape, leading to reduced breach width growth. In our experiment a foreshore reduced the final breach width by 10-20%. Also, we find that the presence of a foreshore has a limiting effect on the specific breach discharge.

Keywords:

Dike, Breach, Discharge, Foreshore, Mid-scale, Experiment

[1]M.vandenBerg-4@tudelft.nl; Delft University of Technology, Delft, The Netherlands
[2]R.J.Labeur@tudelft.nl; Delft University of Technology, Delft, The Netherlands
[3]S.G.J.Aarninkhof@tudelft.nl; Delft University of Technology, Delft, The Netherlands
[4]P.J.Visser@tudelft.nl; Delft University of Technology, Delft, The Netherlands

Research article. **Submitted**: 14 October 2024. **Reviewed**: 21 March 2025. **Accepted** after double-anonymous review: 21 March 2025. **Published:** 30 April 2025.

DOI: 10.59490/jchs.2025.0043

Cite as: van den Berg, M., Labeur, R.J., Aarninkhof, S.G.J., Visser, P.J., Exploring the effect of foreshores on dike breach development via a mid-scale experiment, Journal of Coastal and Hydraulic Structures, 43, DOI: 10.59490/jchs.2025.0043

This paper is part of the **Thematic Series** of selected papers on advances in physical modelling and measurement of Coastal Engineering issues, as presented on the Coastlab Conference in Delft in 2024.

The Journal of Coastal and Hydraulic Structures is a community-based, free, and open access journal for the dissemination of high-quality knowledge on the engineering science of coastal and hydraulic structures. This paper has been written and reviewed with care. However, the authors and the journal do not accept any liability which might arise from use of its contents. Copyright © 2025 by the authors. This journal paper is published under a CC BY 4.0 license, which allows anyone to redistribute, mix and adapt, as long as credit is given to the authors.

1 Introduction

Much of the populated deltas is low-lying area protected by flood defence structures such as seawalls, dunes and dikes (levees), of which the latter are most common and the focus in this study. Flood risk (flood probability times its damage) of these areas is expected to increase substantially due to population growth (Neumann et al., 2015), climate change induced sea level rise (Vitousek et al., 2017; Vousdoukas et al., 2018; Taherkhani et al., 2020), increased storm intensity (Chan et al., 2023), extreme precipitation (Kendon et al., 2014) and ongoing land subsidence (Fang et al., 2022; Tay et al., 2022). Consequently, Almar et al. (2021) estimate that the global aggregated annual overtopping hours for dikes can be up to 50 times larger compared to present-day. Evidently, more overtopping events increase dike failure probability and thus flood risk.

Dikes are frequently strengthened to maintain adequate reliability for flood risk. To aid these conventional methods, Nature-based Solutions such as tidal marshes are increasingly proposed (Temmerman et al., 2013; Narayan et al., 2016; van Wesenbeeck et al., 2017). Tidal marshes are a type of coastal wetland characterised by their elevation near mean high water and regular tidal inundation. They provide important ecosystem services (Barbier et al., 2011), of which one is flood protection. Dikes behind tidal marshes are protected through wave attenuation, reducing failure probabilities (Möller et al., 2014; Vuik et al., 2016). Moreover, tidal marshes can grow with sea level rise via sediment accretion, given the rate of the former does not exceed that of the latter (Stralberg et al., 2011; Morris et al., 2016; Mitchell et al., 2017; Horton et al., 2018; Saintilan et al., 2022). Unfortunately, coastal wetlands are under severe pressure due to land reclamation (poldering) (Scott et al., 2014) and coastal squeeze (Pontee, 2013). Davidson (2014) estimates that over 50% of the global coastal wetland area has been lost since the 20^{th} century, and 87% since the 18^{th} century. Since the 1990's, many restoration techniques have been developed and evaluated (Billah et al., 2022), and shown to reduce flood risk (Taylor-Burns et al., 2024). Zhu et al. (2020) showed that tidal marshes also reduce dike breach growth. Thus, tidal marshes not only reduce flood probability (dike breach) but potentially also flood damage (breach growth).

Generally, flood risk assessment focuses mainly on failure probability of the flood defence. A logical practice, because flood prevention is much preferred over flood damage mitigation from a social economic perspective, especially in vulnerable low-lying (polder) areas. This means that for tidal marshes, research effort is primarily focused on quantifying dike hydraulic load reduction (storm surge and wave impact), and less on quantifying their effect on the dike breaching process (flood damage). Accurate modelling of the breaching process improves breach discharge estimates, which in turn benefits inundation modelling accuracy used in flood damage assessment. In the context of dike breaching, tidal marshes are considered a foreshore, which is seaside land between mean low and high water adjacent to a dike. While other types of foreshores exist, like a mudflat or beach, tidal marshes are generally considered most effective due to their high elevation and relatively stable soil, especially under high flow velocities (Schoutens et al., 2022; Van den Berg et al., 2024; Stoorvogel et al., 2024). Clearly, in view of potential flood damage benefits of foreshores, it is worth studying their effect on the dike breaching process and associated discharge.

According to Visser (1998, 1999) the dike breaching process, given an initial damage at the crest causing overflow (t_0), can be split into five stages (Figure 1): (1) Steepening of the inner slope; (2) Regression of the inner slope; (3) Lowering of the dike crest level in the breach (i.e., breach bottom); (4) Widening of the breach due to critical flow and; (5) Widening of the breach due to subcritical flow. Breach growth stops once flow velocities in the breach no longer cause erosion (end of stage 5, t_6). In stages 1 and 2, development is governed by the erosion of the inner slope and a foreshore effect is negligible. In stage 3, erosion of the inner slope lowers the dike crest in the breach. Once this crest level drops to the foreshore level, further development is affected by the foreshore (erodibility). Yet, how the breaching process is affected from this moment in stage 3 onwards has not been studied yet. ASCE (2011) reports over 726 dike breach experiments since the early 1960's (expanded from Wahl (2007), see also Morris et al. (2009)), but the majority is on small-scale homogeneous dikes (height=0.15-1.0 m), with non-cohesive soils (e.g., sand and rockfill) and without a foreshore. To the authors knowledge, only recently an exploratory small-scale flume experiment was done by van den Hoven et al. (2023) with both erodible and non-erodible foreshores, but under constant breach width conditions. Although they confirmed the discharge reducing effect of foreshores, experiments with a combined erodible foreshore and dike are yet to be done.

In this study we performed multiple dike breach tests to investigate how a foreshore affects dike breach development. At full scale, dikes adjacent to tidal marshes can exceed 6 m in height. In our experiment, the model dike height was scaled to 1.5-1.9 m. Because this scale (1:3-1:4) is larger than typical laboratory scales (1:6 or smaller) but smaller than prototype scale, we consider this a mid-scale experiment. At this scale, flow velocities are sufficiently high to generate hydrodynamic effects such as dilatancy (van Rhee, 2010; Bisschop et al., 2011, 2016), which are difficult to reproduce at smaller scales. The model dike was breached a total seven times, with and without a foreshore present. Two types of foreshores were tested: North Sea sand as a proxy for a sandy (erodible) beach and Dutch river clay as a proxy for a relatively stable (low-erodible) unvegetated tidal marsh.

Flow through a dike breach is typically considered as weir flow, owing to similarities in shape, hydraulic conditions, hydrodynamics and flow control. Firstly, the typical trapezoidal dike profile is found in weir studies (Chen et al., 2018; Zerihun, 2020; Zhang et al., 2023). Secondly, in both scenarios there is a free-surface gravity flow over an obstruction where an upstream subcritical flow becomes critical over the weir and turns into a downstream supercritical flow. The flow is then controlled by the shape of the weir and the upstream hydraulic conditions until downstream water levels sufficiently submerge the weir. Dike breach discharge is then analogous to weir discharge and the following discharge equation applies (Azimi, 2021):

$$Q = C_d \sqrt{g} B \left(\frac{2}{3} h_0 \right)^{3/2} \tag{1}$$

where Q is the weir discharge, C_d the discharge coefficient to correct for non-ideal hydraulic conditions and weir shape, g gravitational acceleration, B weir width and h_0 the upstream water level above the weir (here: breach bottom), assuming h_0 equals the local energy head. We explore foreshore effects on the dike breach development through these parameters and compare the breach shape with historic dike breaches. Our findings are discussed in view of the implications for adapting dike breach models to incorporate foreshore effects.

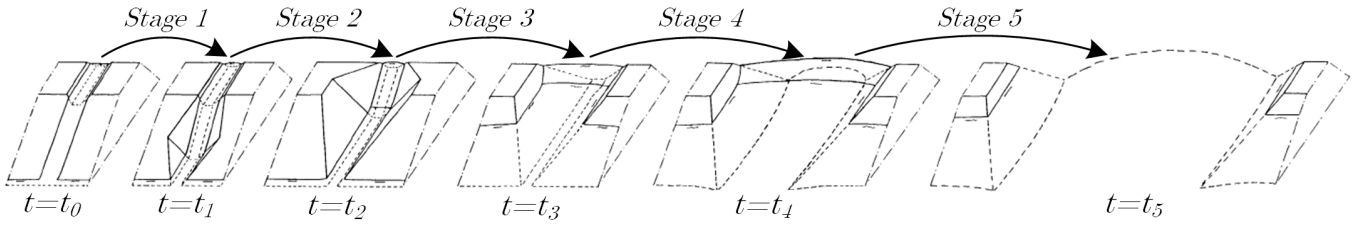

Figure 1: The five-step breach erosion mechanism, adapted from Visser (1998, 1999). Breach stage n is the time interval between t_{n-1} and t_n, where at the end of stage 5 (t_5) breach growth stops and at t_6 flow stops.

2 Experimental setup

2.1 General test setup

The series of dike breach tests was done at Delft University of Technology, at the Flood Proof Holland (FPH) facility of VPdelta+. A 3D representation of the test basin is shown in Figure 2A. This basin is 21 m long, 16.5 m wide and 1.6 m deep. Due to the relatively small size of the basin compared to the expected breach discharge, a pump system was installed to pump downstream water back upstream.

The model dike (Figure 2B) was constructed from three 0.5-0.6 m thick sand layers using a small (5 tonne) excavator. Each layer was compacted using a plate compactor. Once finished, the dike slopes were compacted by pressing the flat end of the excavator bucket onto the slope. Foreshores were built after the dike was completed and consisted of two compacted layers. For the sand foreshore the plate compactor was used, for the clay foreshore the excavator was driven over the top layer for additional compaction.

The sediments used in the experiment are dredged North Sea sand and Dutch river clay. The North Sea sand was delivered in two batches (one for the dike body, one for the sandy foreshore) from different sources in the North Sea, the river clay was used only for the foreshore.

For details about the test basin and pump system, as well as sediment properties and characteristics, we refer to the Appendix A.

2.2 Data collection

Here, only the data collection done during the experiment is outlined. Post-processing is discussed in the Appendix B. A schematised top view of the equipment setup is shown in Figure 3A. Two pressure sensors were installed on each side of the dike to measure upstream (OSSI-010-003C-03) and downstream (Van Essen CTD-Diver DI271) water levels. A fifth pressure sensor (Van Essen CTD-Diver DI271) was used as a barometer to compensate for local air pressure fluctuations.

Four cameras (GoPro Hero10, 1080p@60fps) were used to record the breach growth from the front, back and top (facing upstream and downstream attached to an overhead metal frame). A 1x1m red grid was spray painted on the

inner slope of the dike to measure the breach width when post-processing the footage from the front facing camera.

A 3D laser scanner (Leica ScanStation P40) was used to scan the entire basin at three different positions, before and after a test. From overlaying the scans, breach shape and eroded volumes were determined. Unfortunately, only scans could be done from the tests where a foreshore was present due to scanner availability.

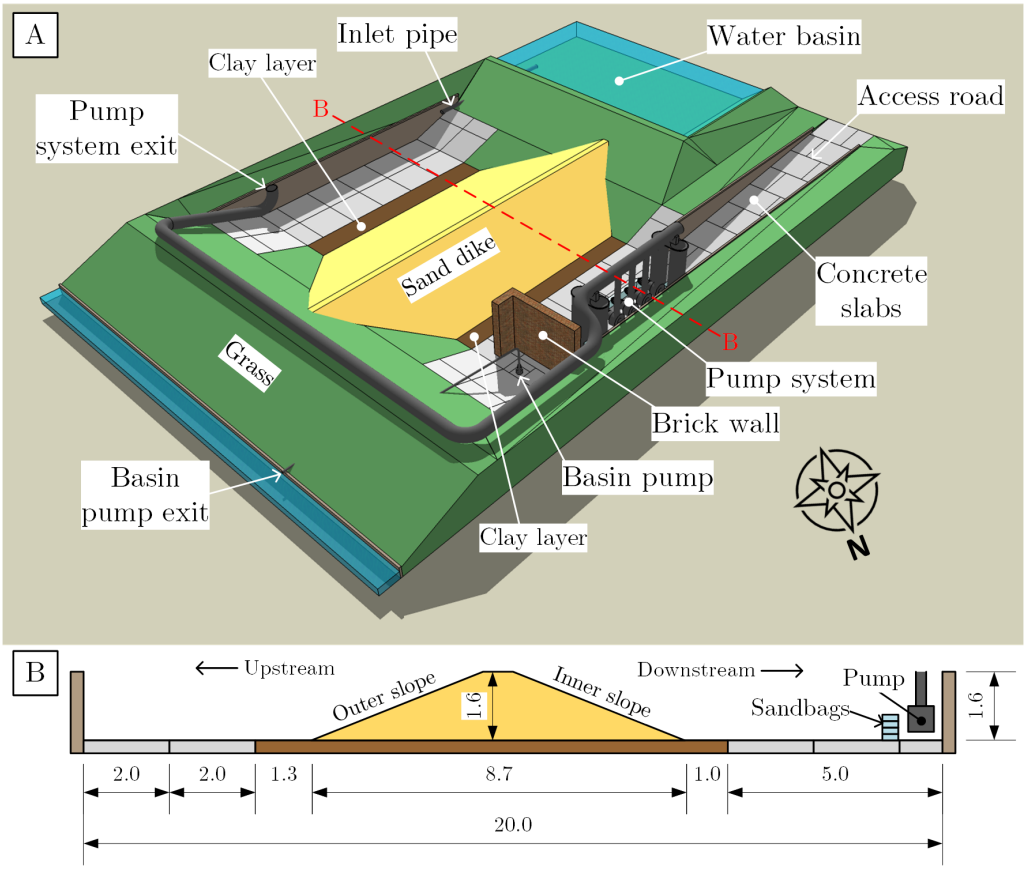

Figure 2: **(A)** 3D model of the experimental setup. **(B)** Scaled schematisation of cross section B-B (length in metres).

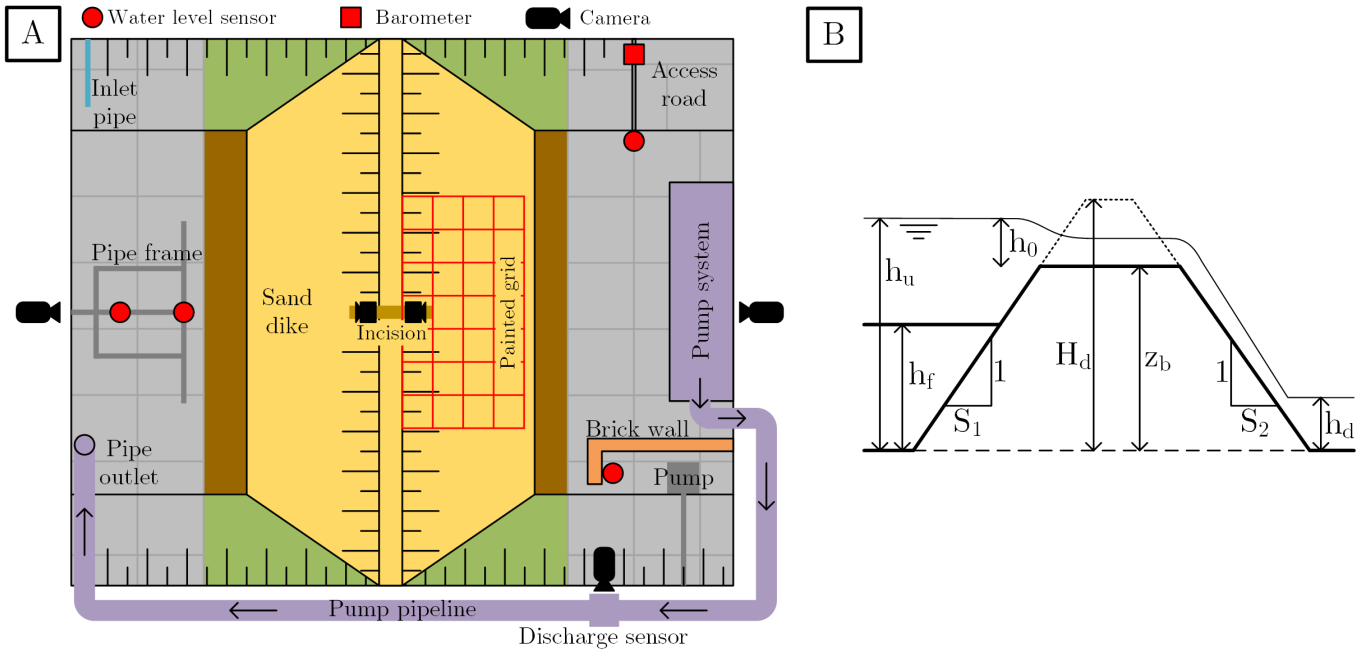

Figure 3: **A** Schematised top view of the equipment setup. The basin width to length ratio is scaled. **B** Schematic of symbols for dike, foreshore and water level parameters varied in this study, see also Section 2.3. Here, the upstream water level h_u, downstream water level h_d, foreshore level h_f, dike height H_d and breach bottom z_b are relative to the basin bottom, h_0 is the upstream water level above the breach bottom z_b and S_1 and S_2 are the outer and inner slope coefficients, respectively.

2.3 Test series

A total of seven tests were done, see Table 1. First, three reference tests (R1-R3) were done without a foreshore. Then, a 0.8 m thick sandy foreshore was added (test S1). Little erosion of the foreshore was observed. To promote erosion, and assumed increased foreshore effects, it was heightened to 1.0 m for the second test S2. Lastly, the sandy foreshore was replaced by a 1.0 m thick clay foreshore (test C1), which had consolidated to a 0.9 m thick layer in test C2. The foreshore tests (S1, S2, C1 & C2) are best compared with the third reference test (R3) because of the equal slope steepness. On the day of test R3 rainfall throughout the day saturated the dike body, and for tests S2 and C2 rainfall in the morning partially saturated the dike body. Sediment saturation reduces the dilatancy effect, increasing erosion rates (Section 3.3). The test procedure is outlined in the Appendix C.

Table 1: Full test series. For a graphic representation of the symbols used, see Figure 3B.

Test	Dike			Foreshore		Initial levels		Breach	Notes
ID	Height H_d [m]	Outer slope S_1 [-]	Inner slope S_2 [-]	Type	Height h_f [m]	Upstream h_u [m]	Downstream h_d [m]	Bottom z_b [m]	
R1	1.55	2.5	3.0	-	-	1.51	0	1.46	Hor. pipe exit
R2	1.55	2.5	3.0	-	-	1.49	0.05	1.45	
R3	1.6	2.5	2.5	-	-	1.48	0.35	1.45	Rain all day
S1	1.7	2.5	2.5	Sand	0.8	1.51	0.23	1.49	
S2	1.7	2.5	2.5	Sand	1.0	1.55	0.22	1.51	Morning rain
C1	1.8	2.5	2.5	Clay	1.0	1.54	0.31	1.51	
C2	1.9	2.5	2.5	Clay	0.9	1.54	0.32	1.50	Morning rain

3 Results

3.1 General breach development

For all tests, the observed breach development corresponds well with the stages described by Visser (1998, 1999). An example is depicted in Figure 4. After initial incision at the crest, flow along the inner slope initiated stage 1. During stage 1, the inner slope steepened and a staircase profile with pools developed where sediment transport capacity (STC) was reached (Figure 4A, see also Appendix D). During stage 2 (Figure 4B), the observed water surface profile was nearly parallel to the initial dike inner slope. This implies that the slope did not steepen much past its initial slope in stage 1 (nor 2), contrary to the prediction by Visser (1998). In accordance with Visser (1998) the breach bottom quickly lowered in stage 3 (Figure 4C), resulting in a rapid increase of flow velocity and breach discharge. The downstream water level rose quickly and, due to the small downstream basin area, above the lowering breach bottom, causing a submerged weir during stage 3 (Figure 4D). The breach bottom continued to decrease, but never eroded to the basin bottom. Thus, stage 4 was skipped and stage 5 was reached (Figure 4E). Stage 5 was short and the test ended when the water levels equalled (Figure 4F). Afterwards, the breach side slopes remained unstable and collapsed (slumping), further increasing the breach width. This increase in breach width and changes to the breach shape were only taken into account in the analysis of the final breach shape (Section 3.4).

During stages 1 and 2, eroded sediment was deposited near the toe of the inner slope, creating a sill (see Figure 4B, submerged from C onwards). This sill can be eroded in stage 3 by increased flow velocity and discharge (sufficient STC). Although this was briefly observed, the quickly increasing downstream water level and limited basin area prevented this mechanism to continue. A small excavator was used to mitigate this somewhat but its reach and capacity were insufficient to have a noticeable affect. The presence of the sill near the toe of the inner slope limited the development of a scour hole in the breach (Section 3.4).

Despite the similarities in the breach development, differences in the duration of the same stage between some tests were observed. These differences could sometimes be related to the foreshore (Section 3.2). For the remainder of the results, the effect of the foreshore on the breach development is evaluated using the weir equation (Equation 1). Changes in hydrodynamics alter the erosion processes in the breach, leading to changes in the breach shape (width B, Section 3.3 and discharge coefficient C_d, Section 3.4 & 3.6). Ultimately, all changes affect the breach specific discharge (q, Section 3.5). Lastly, we compare the observed weir shape with historic breaches in Section 3.7.

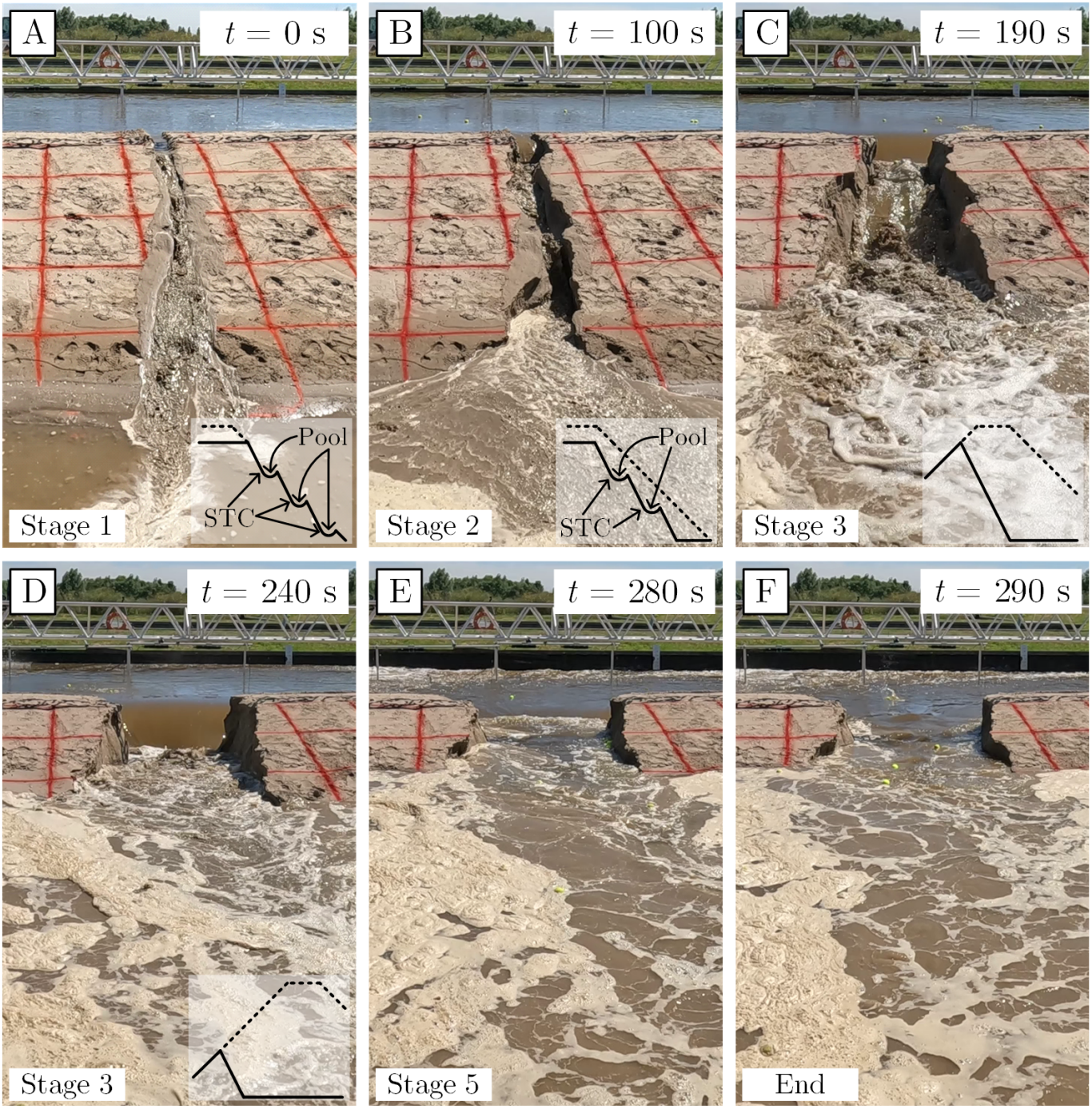

Figure 4: Example of breach development during a test (here: test R2, time (t) is test specific). **(A)** Flow along inner slope in stage 1, where $t = 0$ was when the flow reached the inner toe of the dike. **(B)** Inner slope regression in stage 2. **(C)** Lowering of the breach crest level in stage 3, associated with rapid increase of flow velocity and discharge. **(D)** Continued stage 3, with a clear weir flow upstream and a high downstream water level. **(E)** The weir quickly became drowned (submerged) in stage 3. The breach crest did not erode to the foundation, thus stage 4 is skipped in the test and stage 5 starts. **(F)** End of the test when the upstream and downstream water levels were equal.

3.2 Stage duration

The stage duration is an indication of the development rate of a breach. For the same dike (sediment and geometry) and similar hydraulic boundary conditions, a longer duration indicates a slower erosion process.

Overall, the duration of the same stage between tests was comparable (Table 2, Figure 5), but as mentioned previously with some exceptions. Stage 1 typically took 0:10-0:20 minutes, stage 2 1:50-2:10 minutes, stage 3 2:20-2:40 minutes, stage 4 was skipped (see Section 3.1) and stage 5 took 0:10-0:20 minutes. Duration deviated from this in some tests, depending on the initial dike configuration and the moment the pump system was operational. Firstly, stage 1 for test S1 took 20 seconds longer due to a lower initial h_0 compared to the other tests (Table 1). This led to lower erosion rates on the inner slope, which also resulted in a roughly 1 minute longer stage 2 duration. Furthermore, stage 2 duration for both clay tests (C1 & C2) was around 3 minutes due to a larger initial breach depth ($H_d - z_b$, Table 1), where collapse of the breach side slopes temporarily closed the breach. In stage 3 this collapse was not the cause for a 20-40 seconds longer duration for both clay tests. Instead, this can be related to a combination of a smaller breach width (Section 3.3) and breach shape (Section 3.4) resulting in reduced breach specific discharges (Section 3.5). Lastly, the pump system was operational from the second half of stage 3 onwards (except S2, where this was in stage 5). By then, breach discharge typically exceeded pump capacity, rendering it mostly ineffective (Section 4.1). Only for tests S2, C1 and C2 stage 5 was extended. The extension period relied mainly on when the pumps were stopped, which was earliest for S2 and latest for C1.

Summarising, the effect of a foreshore can be observed in the stage duration. The effect of a foreshore becomes apparent in stage 3, likely once the breach bottom reaches the foreshore level. From this moment, the foreshore starts to affect the hydrodynamics (i.e., h_0). The specific moment t when this occurs in the tests is unknown. Nonetheless, its effect is noticeable for the tests with a stable clay foreshore (C1 & C2) and hints towards a discharge reduction. This is compounded by the fact that the pump system only effectively extended stage 5 for the tests with a sandy or clay foreshore.

Test	Stage					Total
ID	1	2	3	4	5	
R1	0:10	1:50	2:30	-	0:10	4:40
R2	0:10	2:10	2:20	-	0:10	4:50
R3	0:20	2:00	2:40	-	0:20	5:20
S1	0:40	3:10	2:20	-	0:20	6:30
S2	0:20	1:50	2:30	-	1:00	5:40
C1	0:20	2:40	3:00	-	2:20	8:20
C2	0:20	3:30	3:10	-	0:50	7:50

Table 2: Observed stage duration for each test in min:sec.

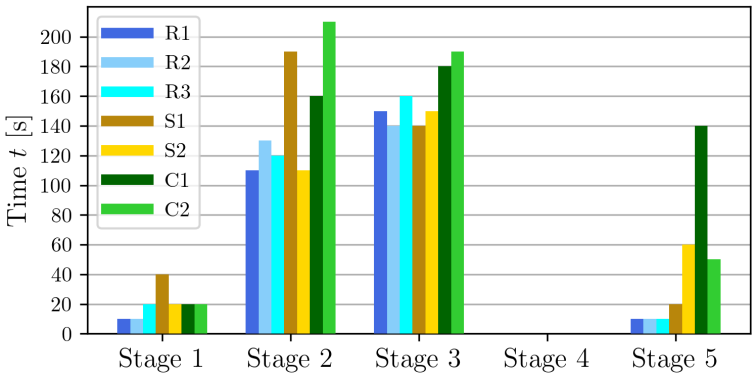

Figure 5: Bar chart of the observed stage duration for each test.

3.3 Breach width growth

Changes in the hydrodynamics alter the erosion processes in the breach which lead to changes in its growth pattern. During the breaching process, the best indication of this is the growth of the breach width (Figure 6).

For all tests the width barely increases during the first two stages, only due to some minor side slope collapse events. This corresponds well with the description of stages 1 and 2 by Visser (1998, 1999), in which no width growth is defined. In the reference tests and test S2 the width increased quickly in stage 3, reaching a maximum growth rate and maintaining this rate throughout the stage before reducing near stage end. However, for tests S1, C1 and C2 lower growth rates were measured at the start of stage 3, then briefly spiked in the second half (notice the sudden large jump in width in Figure 6) before they reduced to values close to zero. In stage 5 growth was negligible for most tests except C1, where further growth was aided by the pump system.

There was a large difference in the final breach width between the first two and third reference tests. This may be attributed to differences in 1) the downstream slope steepness between the tests and 2) dike saturation (Table 1). As mentioned in Section 3.1, the inner slope of the dike did not steepen much. The slope in test R3 was larger than in R1 and R2 leading to higher flow velocities (Figure 7) and consequently higher erosion rates. Secondly, the dike of test R3 was saturated by non-stop rainfall that day. For saturated sand the pores are filled with water instead of air, leading to lower resistance to erosion as the inward pressure gradient when eroded (dilatancy) is reduced. We hypothesise

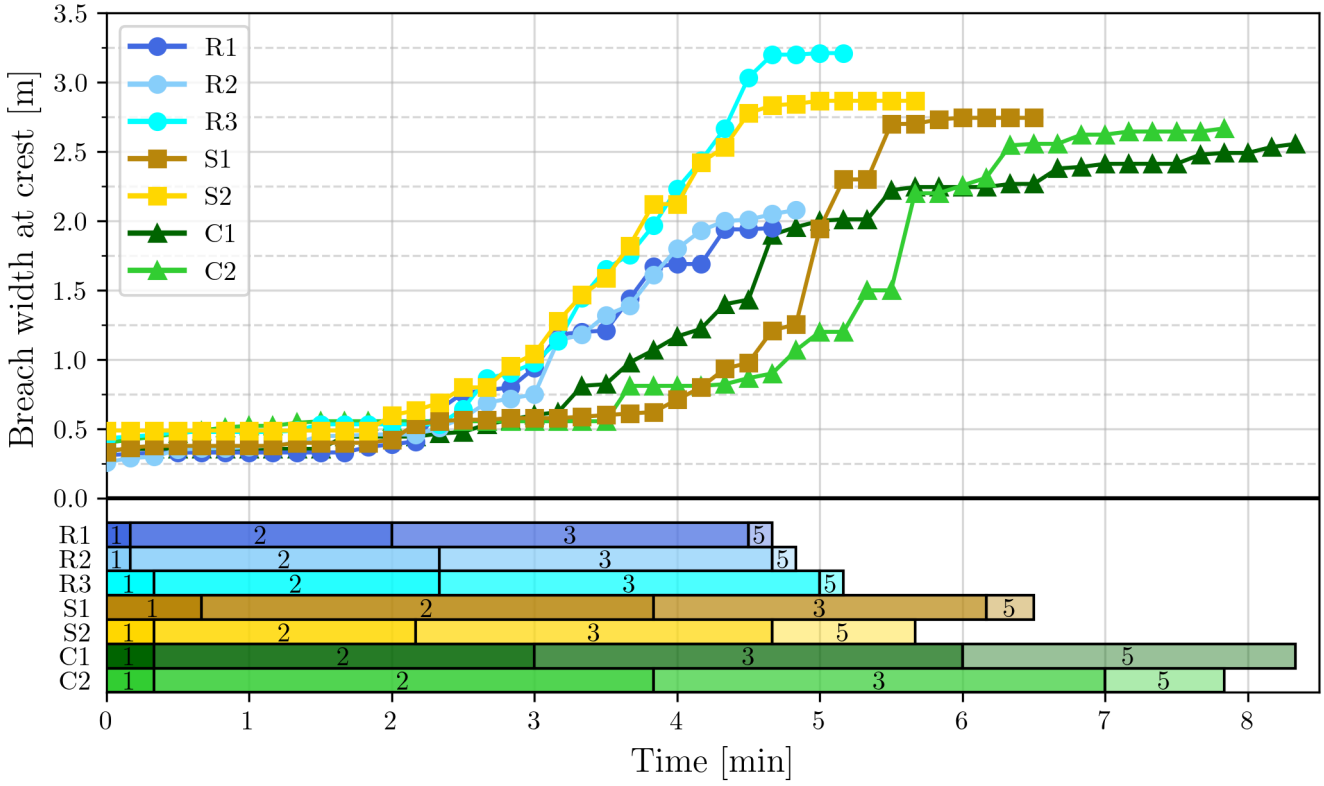

Figure 6: Measured breach widths and growth rate at dike crest at 10 second intervals until test end (i.e., excluding width increase due to slumping after the test ended). The horizontal bar chart shows the recorded stage times (Table 2).

that the downstream slope had a larger effect for these tests as the dike saturation of test S2 was estimated closer to R1 and R2 than R3.

The main differences in breach width growth rates were observed for stage 3. The mean growth rates (Table 3) of stage 3 are lower for the sand and clay foreshore tests compared to R3, respectively 12% and 43% lower. The end of stage 3 has a large impact, where the rates for the foreshore tests are close to zero. This moment before the end of stage 3 occurs sooner for the clay tests (t=1:20 min.) than for the sand tests (t=0:20-0:40 min.) and reference tests (t=0:10-0:20 min.). Further comparing test R3 with the foreshore tests, a decreasing breach width trend with increased foreshore stability can be observed (Table 3). When a sandy or clay foreshore is present, the breach width is on average respectively 14% and 20% smaller.

As observed in Section 3.2, the effect of a foreshore starts in stage 3. In this case this is observed in the rates of breach width growth and final breach width (B). The affected hydrodynamics clearly reduce erosion rates, as for both the sandy and clay foreshore a growth rate reduction was measured. Moreover, again clay foreshores have a larger effect than sandy foreshores.

Table 3: Mean breach growth rate for each stage and final breach width for each test.

Test	Mean breach growth rate [cm s^{-1}]					Final width
ID	Stage 1	Stage 2	Stage 3	Stage 4	Stage 5	[m]
R1	0.10	0.07	0.98	-	0.10	1.95
R2	0.20	0.21	1.05	-	0.30	2.08
R3	0.15	0.14	1.58	-	0.00	3.21
S1	0.09	0.17	1.41	-	0.00	2.74
S2	0.00	0.17	1.38	-	0.05	2.87
C1	0.04	0.16	0.87	-	0.22	2.56
C2	0.22	0.17	0.92	-	0.09	2.67

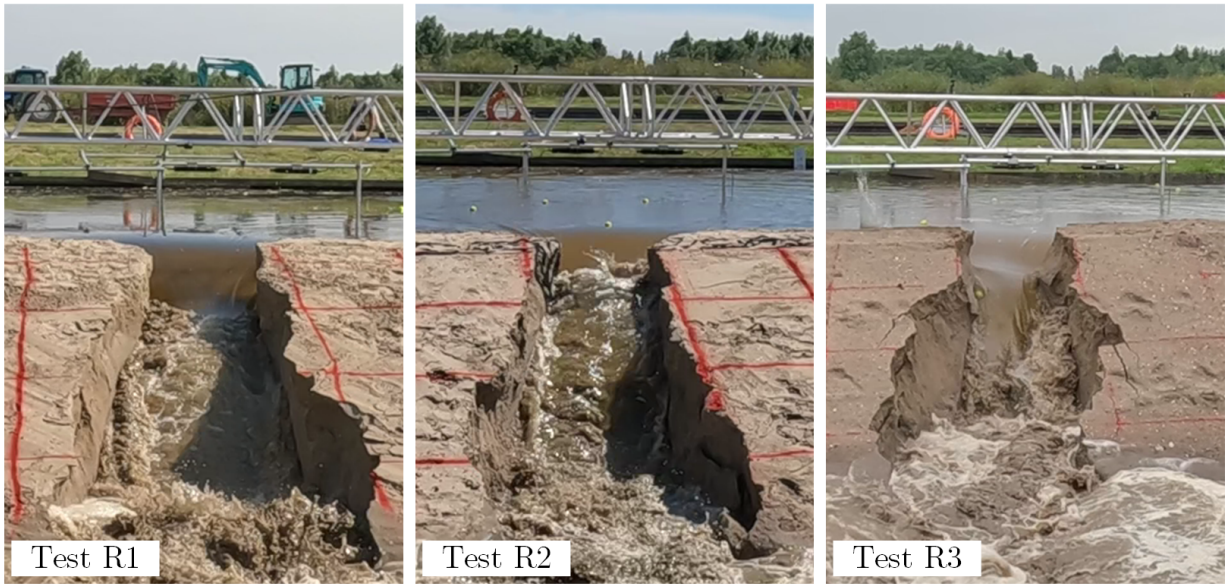

Figure 7: Front of breach of the reference tests at t=3 minutes, highlighting the difference in flow on the dike inner slope.

3.4 Final breach shape

A longer stage 3 duration (Section 3.2) and reduced rates of breach width growth (Section 3.3) were observed when a foreshore was present. As a breach flow can be represented as weir flow, analysis of the final breach shape (Figure 8) reveals foreshore effects on this weir shape.

Visser (1998) defines the breach cross-section as a trapezoid. The initial breach shape (incision at test start) was trapezoidal, but during the tests almost rectangular because the breach side slopes were almost vertical (80-90°). The trapezoidal shape was again observed after the tests (Figure 8C), after breach side slope slumping had occurred while the water in the basin was drained after a test. The angle of the breach side slopes below the equilibrium waterlevel (h=100-110 cm, see Figure 14 in Appendix B) was measured at 25-30°, which is less than the dry internal friction angle of the sediment. Above the equilibrium waterline the breach side slopes remained close to vertical, similar to during a test. The level to where the scour hole in the breach eroded was similar for all tests (0.3-0.4 m including test R3, Figure 8B-C), likely as a result of test duration and the sill (Section 3.1) limiting further development. For test R3 the weir level was lower (≈0.7 m) than the foreshore levels and the weir had a rather elliptical, rounded edge, following local streamlines.

Regarding the weir shape of breaches with a foreshore, most noticeable is the weir edge (Figure 8A). A straight and elliptical weir edge is observed for respective clay and sand foreshores, owing to a stable (low-erodible) clay layer and erodible sand layer. Further, the contour lines near the foreshore edge indicate a steeper slope for the clay than the sandy foreshore (see also Figure 8B). The downstream weir slope for the sand and clay foreshore tests is roughly 15° and 20°, respectively. Similarly to the reference tests, the weir edge of the sand foreshore was rounded, following local streamlines, while an abrupt (headcut like) edge for the tests with a clay foreshore was observed. Also, for the clay foreshore tests the breach has a stronger hourglass shape compared to the sandy foreshore tests (Figure 8A), likely as a result of more horizontal flow contraction.

An effect of the foreshore on the total eroded volume was not observed, see Table 4. The difference between test R2 and the other tests is explained by the smaller breach width and the dike volume per unit width (≈ 7.1 m^3 m^{-1} for H_d=1.55 m). Comparing test R3 with the foreshore tests, a weak decreasing trend may be observed. Similar eroded volumes were achieved after different test duration, indicating slower erosion rates for the tests with a foreshore.

All in all, the effect of a foreshore on the final breach shape is minimal in these tests. For all tests the scour hole developed to a similar degree, and its bottom reached similar levels. The horizontal planar shape showed some resemblance to a hourglass, especially for the clay foreshore tests. Most noticeable was the weir edge shape. For both the reference and sandy foreshore tests the weir edge shape was elliptical as it adjusted to local streamlines, eliminating sharp velocity gradients and associated expansion losses. For the clay foreshore a straight weir edge and small headcut formed where flow detachment likely occurred. These differences in weir edge shape indicate that depending on foreshore presence and stability the weir coefficient C_d is changed.

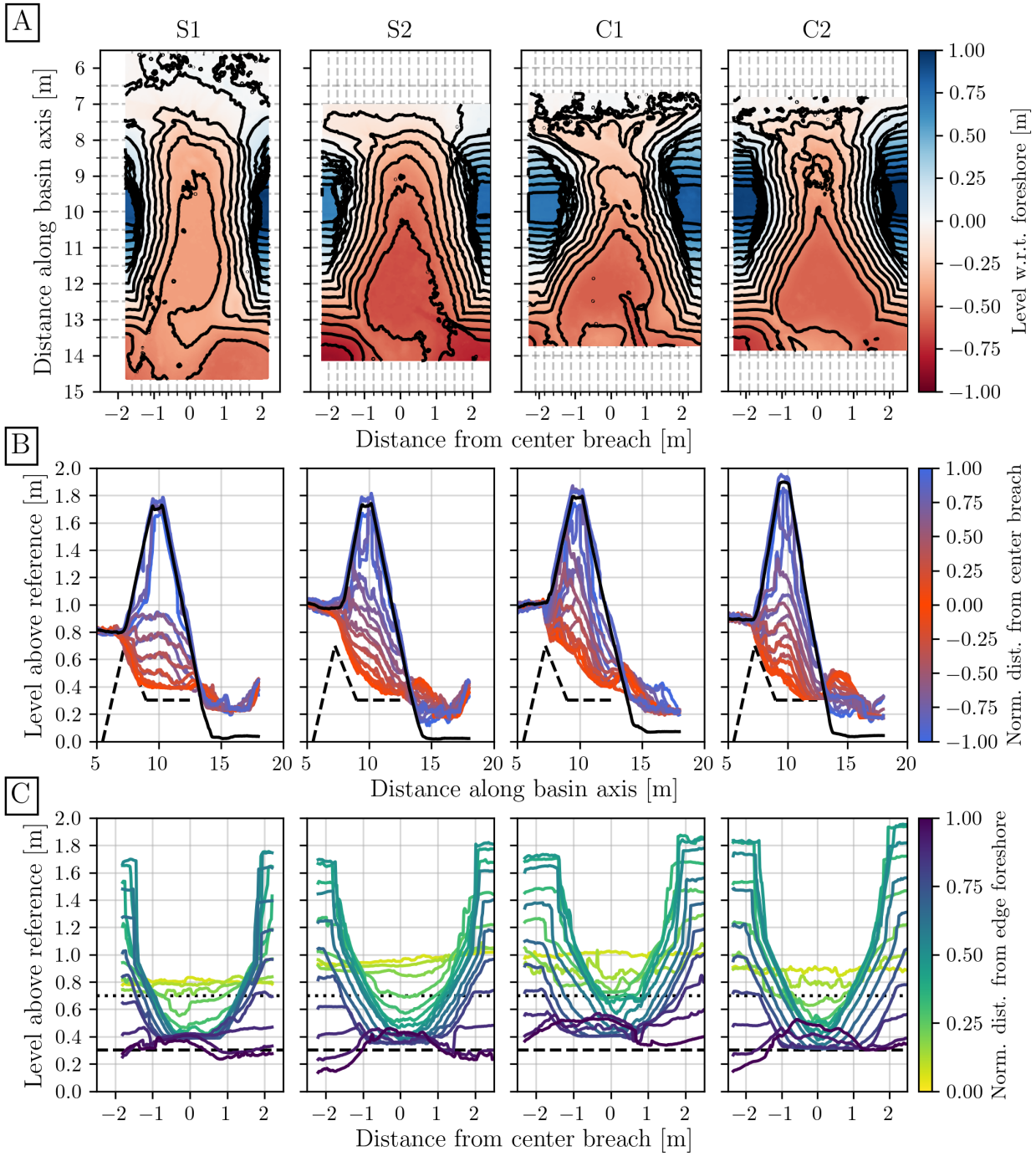

Figure 8: Contours, profiles and cross-sections of the final breach shape for the tests with a foreshore, obtained from the laser scanner. **(A)** Top view contour plot of the final breach shape. Colours show the level of the bed with respect to the foreshore level. The minor x- and y-gridlines represent the locations of the profiles in B and cross-sections in C. **(B)** Breach profiles taken every 0.25 m along the dike axis, including the mean profile before the test in black. The black dashed line represents the schematised breach profile of test R3, excluding the sill. **(C)** Breach cross-sections taken every 0.50 m across the dike axis. The black dotted line represents the weir level of test R3, the black dashed line the breach bottom.

Table 4: Eroded volumes for each test. Volumes for tests Rx were estimated from measured dimensions (R1 could not be determined). Volumes of tests Sx and Cx are computed from the 3D scans, see Section 2.2.

Test	R1	R2	R3	S1	S2	C1	C2
Volume [m^3]	-	7.50	13.89	13.28	12.46	11.49	13.82

3.5 Specific breach discharge

In previous sections the effect of a foreshore on the weir equation parameters (h_0, B and C_d) are discussed, which culminate in changes in the breach discharge Q_{breach}. Because this is dependent on a varying breach width, we focus on the specific breach discharge $q = Q_{breach}/B$ to highlight differences, see Figure 9.

Similarly to the breach width growth in Section 3.3, a large difference is observed between the first two and third reference tests. This discrepancy may be explained by the upstream flow contraction and weir shape. The used breach width at the crest to compute q can be significantly smaller than the width where overflow occurs, see Figure 10. A simple analysis of the overflow width to breach width ratio between the reference tests reveals that this ratio is 1.5-1.6 larger for respectively tests R1 and R2 compared to R3. This would account for at least half of the observed difference in Figure 9. The sand and clay tests closely matched the situation of R3 and can thus be better compared. However, a quantitative comparison remains difficult due to the sensitivity of the result to both the estimated breach width and basin storage area.

Regardless, the effect of a foreshore on the discharge can be observed from the general shape of the graphs in Figure 9. Firstly, the maximum gradient in stage 3 is largest for the reference tests, followed closely by test S1, while for tests S2 and both clay tests this gradient is lower. This is the first indication that the foreshore is reducing the specific discharge. The second indication is that for the foreshore tests the specific discharge appears to stabilise once a maximum is reached (S1: t=4:40-5:30 min., S2: t=3:40-4:10 min., C1: t=4:10-5:20 min. and C2: t=5:00-5:50 min.). This strongly suggests that in stages 1 and 2, $h_0 = h_u - z_b$, but once z_b drops below h_f in Stage 3, $h_0 = h_u - h_f$. The hydrodynamics in the breach are then not only dependent on dike erosion, but also foreshore stability. Consequently, the specific discharge is then also limited.

To conclude, with just a qualitative analysis it is revealed that a foreshore can limit the specific breach discharge, which is caused by the foreshore becoming the weir instead of the dropping breach bottom. Essentially, this mechanism results in a limitation of h_0 once the breach bottom drops below the foreshore level. A weak trend may be observed in the comparison between test R3 and the foreshore tests. If the foreshore stability or foreshore level had the largest impact in reducing the specific discharge between the foreshore tests is difficult to determine. Nonetheless, it is likely that for longer test duration and equal initial foreshore level, a clay foreshore is more effective due to its lower erodibility.

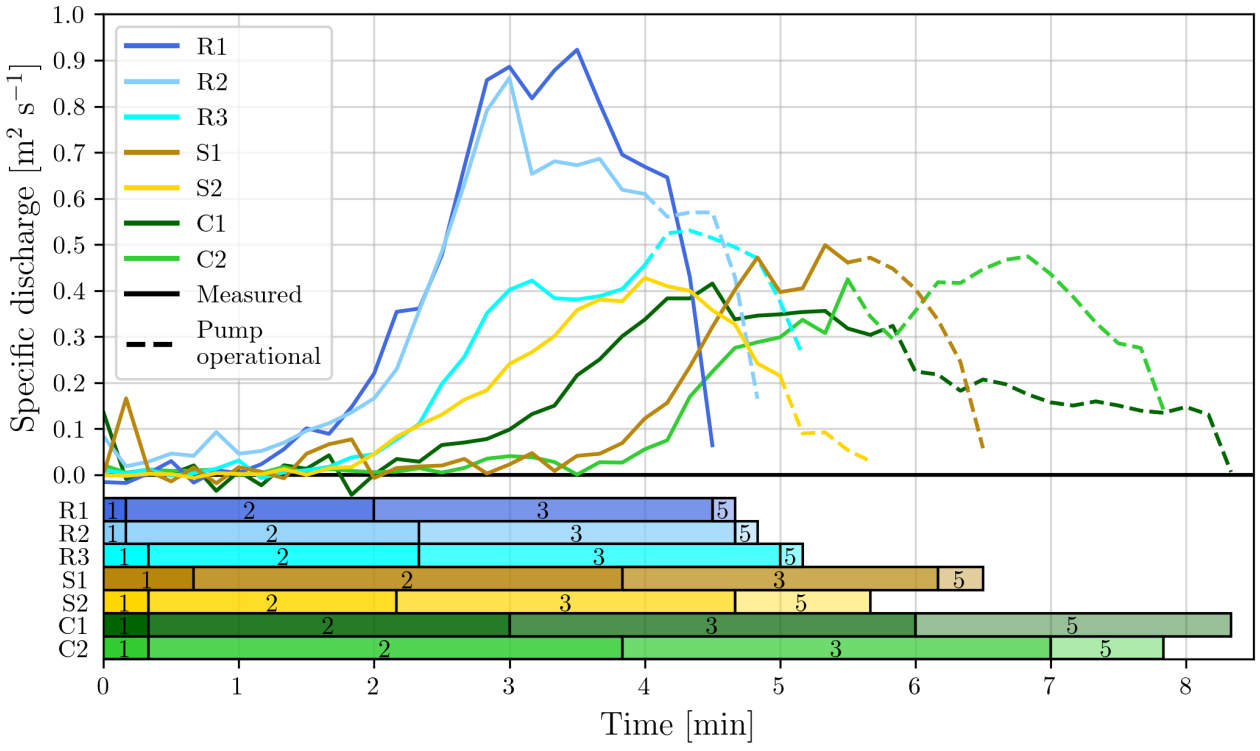

Figure 9: Calculated specific breach discharge q in m^2 s^{-1} for each test. The horizontal bar chart shows the recorded stage times (Table 2).

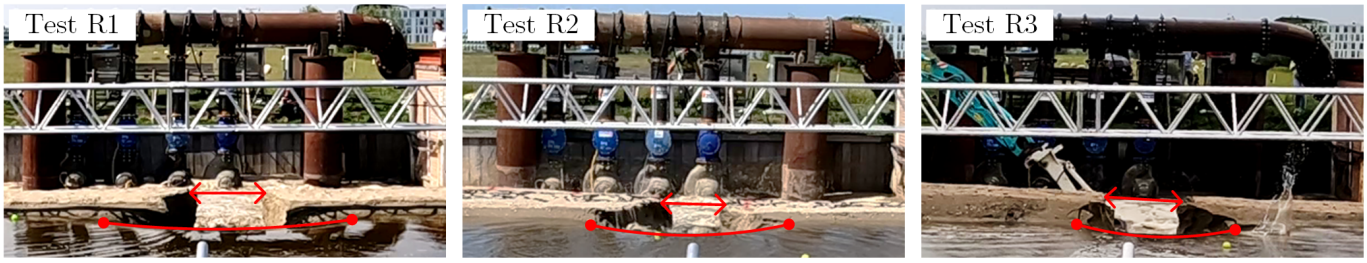

Figure 10: Back of the breach of the reference tests at t=3 minutes (see also Figure 6), highlighting the breach width at dike crest (arrow) and weir width where overflow occurs (curve).

3.6 Estimating the discharge coefficient

Using the calculated specific breach discharge C_d can be estimated, assuming that $h_0 = h_u - h_f$ holds in the period where it stabilises in the foreshore tests. Surprisingly, C_d is then increasing in time for all foreshore tests, starting from 0.5-0.8 and increasing to 1.2-1.6, except for C2 where it ranged from 0.4 to 0.6. Clearly, such a simple analysis does not capture all aspects associated with C_d. Nonetheless, the values are largely in range of what is typical for weirs. Moreover, for the test where the specific discharge stabilises for the longest period, test C2, the range is relatively small and comparable to broad- or long-crested weirs. Generally, coefficients are lower for broad-crested weirs than for short-crested weirs (Azimi and Rajaratnam, 2009), but a streamlined crest (Bagheri and Kabiri-Samani, 2020) and upstream- and downstream slopes (Chen et al., 2018) can significantly impact this. Without a foreshore, the weir shape in stage 3 can be considered a trapezoidal short-crested weir with a circular crest. With a sandy or clay foreshore a broad- or long-crested weir can be considered with respectively a downstream slope or vertical edge. Thus, the weir equation appears to hold for the case that a foreshore is present, but to express this solely in one coefficient requires more research.

3.7 Comparison with historic breach data

The observed weir shapes for the sandy and clay foreshores tests (Section 3.4) are also found in historic breaches from the 1953 North Sea Flood disaster (Watersnoodramp) in southwestern Netherlands (Rijkswaterstaat and KNMI, 1961). Precise measurements of the weir shape are not given, but these can be reconstructed from the provided breach cross-sections and descriptions. At each of the breaches in Figure 11 the maximum seaside waterlevel (h_0) was roughly 2.5 m above the ground level of the foreshore. Ignoring friction, the maximum critical flow velocity can be calculated with $\sqrt{gh_0} \approx 4$ m s^{-1}. When a sandy foreshore is present (Figure 11A), a deep scour hole is found with a gentle downstream weir slope, while for a clay foreshore (Figures 11B and 11C) the scour hole is shallower and the downstream weir slope steep. A more shallow scour hole was not observed in our experiment, probably because the duration of stage 3 was insufficient to observe significant differences. The steeper downstream weir slope for a clay foreshore has also been observed in this study, making it likely a head-cut has formed in both cases. Apparently, research into these historic breaches in relation to foreshores is valuable to better assess performance of scaled experiments to full-scale.

4 Discussion

4.1 Evaluation of the experimental setup and test series

The aim of the experiment was to study how a foreshore affects sand-dike breach development throughout the five stages defined by Visser (1998, 1999). In the experiment, stages 1 and 2 of the breach process were completed, stage 3 partially completed and stage 5 was briefly observed. In stage 3, the eroded sediment created a sill near the inner toe of the dike which suppressed scour hole development (Section 3.4). The use of the small excavator to mitigate this was largely ineffective. The extent to which the sill negatively impacted breach development is difficult to determine. As the same situation was observed across all tests the relative effect between tests is likely small but the absolute effect may not be negligible. The main aspect to consider is the downstream basin size. The available space from a larger downstream basin area reduces the rate at which the water level rises. This promotes sediment transport further away from the breach exit and avoids sediment to build up against the basin walls. This assumes that upstream the flow velocities continue to increase throughout stage 3 as the upstream water level remains constant and the breach bottom drops. In the experiment the upstream water level dropped quickly, thus also a larger upstream basin area

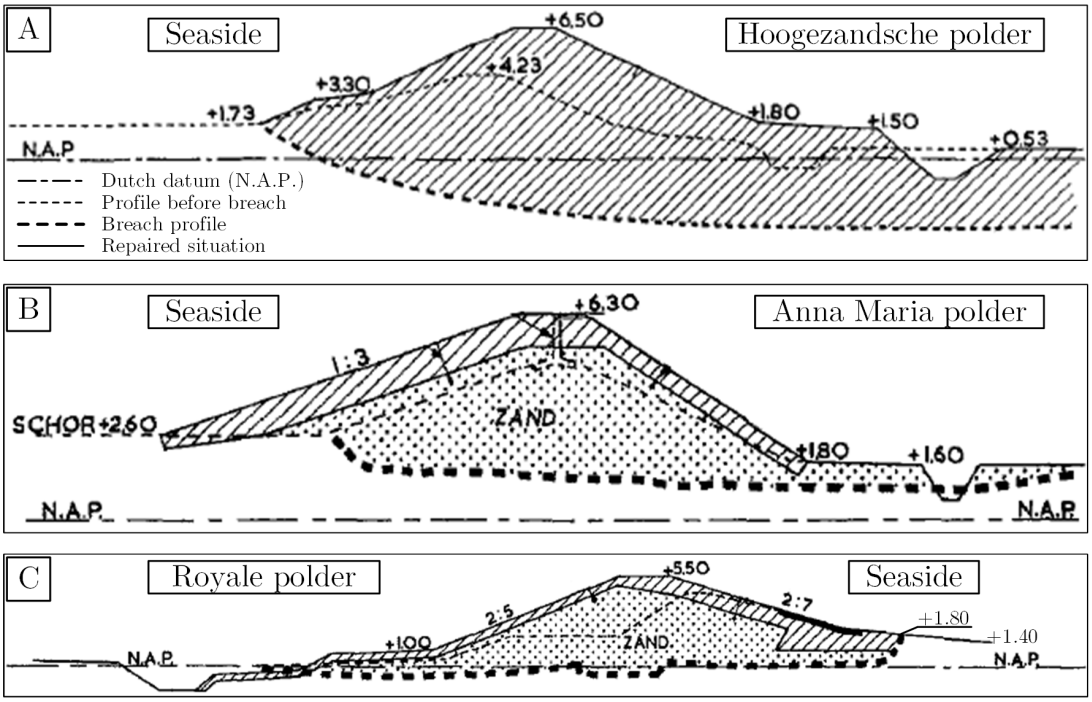

Figure 11: Breach cross-sections from the 1953 North Sea Flood disaster (Watersnoodramp) in southwestern Netherlands, adopted and adapted from Rijkswaterstaat and KNMI (1961). **(A)** Breach at Hoogezandsche polder, with a sandy foreshore at +1.73 m; the position of the cross-section was likely close to a breach side. **(B)** Breach at Anna Maria polder, with a clay foreshore (Dutch *schor* = tidal marsh) at +2.60 m; the position of the cross-section was in the middle of the breach. **(C)** Breach at Royale polder, with a clay foreshore at +1.40 m; the position of the cross-section was in the middle of the breach.

would improve scour hole development. Despite the limited basin size in this study, foreshore effects on the breach development were observed in stage 3. Therefore, for future research a relatively larger basin allows for all stages to develop undisturbed, where emphasis should be on completion of stage 3 and reaching (an approximate) constant progression of stage 4.

The model dike was 1.5-1.9 m high and the foreshore layer thickness between 0.8 and 1.0 m. With a scale of 1:3-1:4 this translates to respectively dike crest and foreshore levels between 6-8 m and 3-4 m above the dike toe (here: basin bottom). Separately, these levels are realistic but the ratio of dike height to foreshore height should also be considered. In this experiment the ratio was around 2.0, while at full scale this ratio is generally higher, especially for coastal dikes. The ratio in this experiment was necessary to promote foreshore effects due to the limited basin size. Thus, the moment the foreshores in the relatively small basin impact the breach development at full scale is relatively later in stage 3 than observed in the tests. Furthermore, the observed general breach development in this study (Section 3.1) corresponds well with observations in other studies at a similar scale or larger. Firstly, ASCE (2011) cite sources of historic dam failures where the trapezoidal final breach shape was also observed, while a rectangular shape (sometimes with side slope undermining) was observed during experiments. Also, the more hourglass shape of the breach (when viewed from the top) observed for the tests with a clay foreshore (C1 & C2) was also observed in experiments with a full clay dike of similar height (Hanson et al., 2005).

The model dike in this study had no clay (cover) layer unlike a full-scale dike. It was assumed that the clay layer was removed in the breach initiation process, as observed in the 1953 North Sea Flood in southwestern Netherlands (Rijkswaterstaat and KNMI, 1961). The investigation of the complicated breach initiation process has not been the aim of this study. Moreover, in stages 3 and 4 erosion of the dike core (here: sand) is dominant in the breaching process due to the high flow velocities and breach side slope collapse (slumping).

To mitigate large water level change rates a pump system was installed to pump downstream water back upstream. The system was only successful in stage 5 due to its operational requirements and above mentioned limited basin size. The required water level to start the system (50 cm above basin bottom) was halfway the equilibrium water level at the end of a test, and was reached in stage 3 where the breach discharges were largest. Although once started the system was typically operational after 30 seconds, by then either the water level difference over the breach was either small or the breach discharge exceeded system capacity. The system can be improved by using pumps of different sizes

such that smaller pumps can start at lower water levels. Nonetheless, one should take into account that at these scales the breach discharge easily reaches several $m^3\ s^{-1}$, exceeding most affordable pump system capacities. If a pump system is desirable or necessary, a separate system for the upstream and downstream basin may be more effective as this allows independent operation and more varied pump types and sizes. Lastly, basins with a sufficiently large area circumvent the necessity of a pump system, which is both financially and operationally beneficial.

Mid-scale experiments require a significant time investment, where the actual test duration is much shorter than the preparation and reconstruction period. Between tests of the same type (no, sand or clay foreshore) little differences were observed in breach development, specific discharge, eroded volumes and breach shape. Main differences were observed in dike profile (tests R1 & R2 compared to R3) and foreshore type (tests Sx & Cx compared to Rx). Therefore, many test repetitions of identical tests may not be time efficient. Varying parameters such as water levels, dike profile, foreshore level and type, and sediment characteristics (dike and foreshore) appear more valuable to study the more general effect of foreshores on dike breach development.

4.2 Implications for dike breach modelling

Dike breach modelling is usually done in either of three ways, with increasing complexity: 1) parametric, 2) simplified physically-based or 3) detailed physically-based, for thorough overviews see Zhu (2006); Morris et al. (2009); Peeters et al. (2011); ASCE (2011); Zhao (2016). Due to their simplicity, parametric models are easiest to adapt and calibrated but require a broad dataset to validate. Simplified physically-based models will require more known input parameters but in turn have increased accuracy. By extension, detailed physically-based models are most accurate but require in-depth theory to be sufficiently reliable. Including foreshores in models will entail additional geotechnical sediment characteristics and knowledge on alteration to the hydrodynamics. Considering the accuracy for flood risk assessment and complex hydrodynamics when a foreshore is introduced, especially in case of headcut formation, make parametric and simplified physically-based models likely most suitable to adapt.

Regardless, adapting dike breach models to cope with foreshores boils down to two main factors: foreshore stability and its effect on dike erosion processes. As shown in this study, noticeable foreshore effects occur in stage 3 onwards. During stage 3 the supercritical flows primarily deepen the scour hole while in stage 4 streamwise expansion of the scour hole can be observed (Visser, 1998). Changes in hydrodynamics by the presence and stability of a foreshore can affect this scour hole development. The first signs of this have been observed in this study, where the downstream slope of the weir (i.e., upstream slope of the scour hole) changes depending on foreshore stability (Section 3.4). Continued development in stage 3 and throughout stage 4 may show larger differences due to foreshore stability as seen in historic breaches (Section 3.7). A sandy foreshore is easily eroded and its bed adapts to the streamlines, while a clay foreshore (e.g., tidal marsh) remains relatively stable and develops a headcut. Adaptation of dike breach models for foreshores should thus take foreshore stability and its associated erosion processes into account. In this regard, data from this study can be used as a stepping stone to calibrate or validate existing and adapted dike breach models. However, in light of flood risk modelling the focus is typically on the breach discharge. As shown in this study, foreshores have a specific discharge reducing effect (Section 3.5). Efforts to incorporate foreshore effects in dike breach modelling are therefore best put towards accurate modelling of the discharge effect. Nonetheless, accurate modelling of breach width, depth and foreshore erosion should not be overlooked because this also gives insight into the potential emergency measures and necessary repair works after a dike has breached, which benefits flood risk assessment.

5 Conclusions

Flood risk (flood probability times damage) is increasing due to climate change, sea level rise and land subsidence. Conventional methods to strengthen flood defence infrastructure might no longer suffice and additional strategies such as Nature-based Solutions (NbS) are explored. One of these NbS are coastal wetlands such as tidal marshes. Their benefit to reduce dike breach probability has been well studied. However, their effect on flood damage has been largely overlooked. This effect is related to changes in dike breach development by the presence of a foreshore (e.g., beach/sandy wetland or tidal marsh). To start bridging this knowledge gap we performed a series of mid-scale breach tests where we breached a model sand-dike without a foreshore and with a sandy or clay foreshore. We evaluated foreshore effects using the weir equation typically applied to breach flow. Our results show that the presence of a foreshore alters the weir hydrodynamics, leading to reduced erosion rates and thus breach width. Both a sandy and clay foreshore reduce erosion rates, but the less erodible clay is more effective. Depending on foreshore type, the weir shape is also altered which leads to changes in the discharge coefficient. A sandy foreshore erodes to adapt to local streamlines, creating an elliptical weir edge, while a less erodible clay foreshore creates a straight headcut-like edge. Once clay foreshores significantly erode (not observed in this study), they will also exhibit an elliptical shape, but with

a significantly smaller minor axis compared to the case of a sandy foreshore. These changes culminated in a reduced breach specific discharge (discharge per unit breach width) for both sandy and clay foreshores. Moreover, a breach specific discharge maximum was observed in stage 3 (of the breaching process) for the tests with a sandy and clay foreshore, while without a foreshore the specific discharge only increased. This is mid-scale experimental confirmation that foreshores have a specific discharge reducing effect during a dike breaching event. We also estimated the discharge coefficient and confirmed that the weir equation may still hold when a foreshore is present, but requires more research for true quantification. The overall observations and results from this study give insight into how foreshores affect dike breach development and further highlight their potential to reduce flood damage. Lastly, the results and acquired dataset aid adaptation and validation of (dike breach) models for scenarios with foreshores.

Acknowledgements

We thank Lindsey Schwidder and Jean-Paul de Garde from VPDelta+ for allowing us to use their facility Flood Proof Holland and for their advice and coordination. Thank you Michael Gros from Rental Pump B.V. and his colleagues for their flexibility and quick communication around the pump system. Also, we thank Pieter van der Gaag, Arno van Doorn and Arie van der Vlies for helping with preparation and installation of the measurement equipment. Our gratitude goes to Boskalis N.V. and Zandhandel Schiehaven Delft from Van der Waal B.V. for providing all the required sediment volumes for the experiment. A big thank you to Loonbedrijf van der Ent for their flexibility and expertise on transporting the sediment on site and building and repairing the test dike. A big thank you to Peter Herman who was part of funding acquisition and conceptualisation of this study but is now retired. Lastly, we thank Stephan Rikkert for his contributions during conceptualization and investigation.

Funding

This study is part of the project: *The Hedwige-Prosper Polder as a future-oriented experiment in managed realignment: integrating saltmarshes in water safety* (Project number: 17589) of the research programme **Living Labs in the Dutch Delta** which is (partly) financed by the Dutch Research Council (NWO).

Author contributions (CRediT)

MB: Writing – original draft, Conceptualization, Methodology, Investigation, Data curation, Formal analysis, Validation, Visualisation.

RL: Manuscript draft review and editing.

SA: Manuscript draft review and editing, Conceptualization, Funding acquisition.

PV: Manuscript draft review and editing.

Data access statement

The post-processed data presented in this article, including raw video footage of the experiment is available at 4TU Research Data. DOI:10.4121/b0a3dc96-d373-4012-96fe-7f6963e74f98. For the raw data, please contact the corresponding author.

Conflict of interest (COI)

There is no conflict of interest.

Notation

Name	Symbol	Unit
Basin storage area	A	m^2
Weir (breach) width	B	m
Cohesion	c	kPa
Coefficient of curvature	C_c	-
Weir discharge coefficient	C_d	-
Coefficient of uniformity	C_u	-
10^{th} percentile particle diameter of a sieve analysis	D_{10}	mm
50^{th} percentile (median) particle diameter of a sieve analysis	D_{50}	mm
90^{th} percentile particle diameter of a sieve analysis	D_{90}	mm
Gravitational acceleration	g	m/s^2
Water level above the basin bottom	h	m
Downstream water level above the basin bottom	h_d	m
Foreshore level above the basin bottom	h_f	m
Upstream water level above the basin bottom	h_u	m
Upstream water level above the weir (breach bottom)	h_0	m
Dike height above basin bottom	H_d	m
Sediment permeability	k	m/s
Sediment porosity	n	-
Dike outer slope coefficient	S_1	-
Dike inner slope coefficient	S_2	-
Time	t	s
End of stage n of the breaching process	t_n	s
Weir (breach) discharge	Q	m^3/s
Specific breach discharge	q	m^2/s
Breach bottom above basin bottom	z_b	m
Internal friction angle of the sediment	ϕ	degrees

Abbreviations

FPH Flood Proof Holland

NbS Nature-based Solution

STC Sediment Transport Capacity

References

Almar, R., Ranasinghe, R., Bergsma, E.W.J., Diaz, H., Melet, A., Papa, F., Vousdoukas, M., Athanasiou, P., Dada, O., Almeida, L.P. and Kestenare, E. (2021). A global analysis of extreme coastal water levels with implications for potential coastal overtopping. *Nature Communications*, **12**(1), 3775. ISSN 2041-1723. DOI:10.1038/s41467-021-24008-9.

ASCE (2011). Earthen Embankment Breaching. *Journal of Hydraulic Engineering*, **137**(12), 1549–1564. ISSN 0733-9429. DOI:10.1061/(ASCE)HY.1943-7900.0000498.

Azimi, A.H. (2021). An introduction to hydraulic structures, In: *Water Engineering Modeling and Mathematic Tools*, 297–342, Elsevier.

Azimi, A.H. and Rajaratnam, N. (2009). Discharge Characteristics of Weirs of Finite Crest Length. *Journal of Hydraulic Engineering*, **135**(12), 1081–1085. ISSN 0733-9429. DOI:10.1061/(ASCE)HY.1943-7900.0000117.

Bagheri, S. and Kabiri-Samani, A. (2020). Overflow characteristics of streamlined weirs based on model experimentation. *Flow Measurement and Instrumentation*, **73**, 101720. ISSN 09555986. DOI:10.1016/j.flowmeasinst.2020.101720.

Barbier, E.B., Hacker, S.D., Kennedy, C., Koch, E.W., Stier, A.C. and Silliman, B.R. (2011). The value of estuarine and coastal ecosystem services. *Ecological Monographs*, **81**(2), 169–193. ISSN 1557-7015. DOI:10.1890/10-1510.1.

Billah, M.M., Bhuiyan, M.K.A., Islam, M.A., Das, J. and Hoque, A.R. (2022). Salt marsh restoration: an overview of techniques and success indicators. *Environmental Science and Pollution Research*, **29**(11), 15347–15363. ISSN 0944-1344. DOI:10.1007/s11356-021-18305-5.

Bisschop, F., Miedema, S.A., Visser, P.J., Keetels, G.H. and van Rhee, C. (2016). Experiments on the Pickup Flux of Sand at High Flow Velocities. *Journal of Hydraulic Engineering*, **142**(7). ISSN 0733-9429. DOI:10.1061/(ASCE)HY.1943-7900.0001142.

Bisschop, F., Visser, P.J., Van Rhee, C. and Verhagen, H.J. (2011). Erosion due to high flow velocities: a description of relevant processes. *Coastal Engineering Proceedings*, **1**(32), 24. ISSN 2156-1028. DOI:10.9753/icce.v32.sediment.24.

Chan, S.C., Kendon, E.J., Fowler, H.J., Kahraman, A., Crook, J., Ban, N. and Prein, A.F. (2023). Large-scale dynamics moderate impact-relevant changes to organised convective storms. *Communications Earth & Environment*, **4**(1), 8. ISSN 2662-4435. DOI:10.1038/s43247-022-00669-2.

Chen, Y., Fu, Z., Chen, Q. and Cui, Z. (2018). Discharge Coefficient of Rectangular Short-Crested Weir with Varying Slope Coefficients. *Water*, **10**(2), 204. ISSN 2073-4441. DOI:10.3390/w10020204.

Dafalla, M.A. (2013). Effects of Clay and Moisture Content on Direct Shear Tests for Clay-Sand Mixtures. *Advances in Materials Science and Engineering*, **2013**, 1–8. ISSN 1687-8434. DOI:10.1155/2013/562726.

Davidson, N.C. (2014). How much wetland has the world lost? Long-term and recent trends in global wetland area. *Marine and Freshwater Research*, **65**(10), 934. ISSN 1323-1650. DOI:10.1071/MF14173.

De Battisti, D., Fowler, M.S., Jenkins, S.R., Skov, M.W., Rossi, M., Bouma, T.J., Neyland, P.J. and Griffin, J.N. (2019). Intraspecific Root Trait Variability Along Environmental Gradients Affects Salt Marsh Resistance to Lateral Erosion. *Frontiers in Ecology and Evolution*, **7**. ISSN 2296-701X. DOI:10.3389/fevo.2019.00150.

Fang, J., Nicholls, R.J., Brown, S., Lincke, D., Hinkel, J., Vafeidis, A.T., Du, S., Zhao, Q., Liu, M. and Shi, P. (2022). Benefits of subsidence control for coastal flooding in China. *Nature Communications*, **13**(1), 6946. ISSN 2041-1723. DOI:10.1038/s41467-022-34525-w.

Hanson, G.J., Cook, K.R. and Hunt, S.L. (2005). Physical Modeling of Overtopping Erosion and Breach Formation of Cohesive Embankments. *Transactions of the ASAE*, **48**(5), 1783–1794. ISSN 2151-0059. DOI:10.13031/2013.20012.

Horton, B.P., Shennan, I., Bradley, S.L., Cahill, N., Kirwan, M., Kopp, R.E. and Shaw, T.A. (2018). Predicting marsh vulnerability to sea-level rise using Holocene relative sea-level data. *Nature Communications*, **9**(1), 2687. ISSN 2041-1723. DOI:10.1038/s41467-018-05080-0.

Kendon, E.J., Roberts, N.M., Fowler, H.J., Roberts, M.J., Chan, S.C. and Senior, C.A. (2014). Heavier summer downpours with climate change revealed by weather forecast resolution model. *Nature Climate Change*, **4**(7), 570–576. ISSN 1758-6798. DOI:10.1038/nclimate2258.

Kohsiek, L.H.M. (1984). De korrelgrootte karakteristiek van de zeereep (stuifdijk) langs de Nederlandse kust, Technical Report WWKZ-84G.007, Rijkswaterstaat.

Lo, V., Bouma, T., van Belzen, J., Van Colen, C. and Airoldi, L. (2017). Interactive effects of vegetation and sediment properties on erosion of salt marshes in the Northern Adriatic Sea. *Marine Environmental Research*, **131**, 32–42. ISSN 01411136. DOI:10.1016/j.marenvres.2017.09.006.

Malizia, J.P. and Shakoor, A. (2018). Effect of water content and density on strength and deformation behavior of clay soils. *Engineering Geology*, **244**, 125–131. ISSN 00137952. DOI:10.1016/j.enggeo.2018.07.028.

Marin-Diaz, B., Govers, L.L., van der Wal, D., Olff, H. and Bouma, T.J. (2022). The importance of marshes providing soil stabilization to resist fast-flow erosion in case of a dike breach. *Ecological Applications*, **32**(6). ISSN 1051-0761. DOI:10.1002/eap.2622.

Mitchell, M., Herman, J., Bilkovic, D.M. and Hershner, C. (2017). Marsh persistence under sea-level rise is controlled by multiple, geologically variable stressors. *Ecosystem Health and Sustainability*, **3**(10). ISSN 2096-4129. DOI:10.1080/20964129.2017.1396009.

Möller, I., Kudella, M., Rupprecht, F., Spencer, T., Paul, M., van Wesenbeeck, B.K., Wolters, G., Jensen, K., Bouma, T.J., Miranda-Lange, M. and Schimmels, S. (2014). Wave attenuation over coastal salt marshes under storm surge conditions. *Nature Geoscience*, **7**(10), 727–731. ISSN 1752-0894. DOI:10.1038/ngeo2251.

Morris, J.T., Barber, D.C., Callaway, J.C., Chambers, R., Hagen, S.C., Hopkinson, C.S., Johnson, B.J., Megonigal, P., Neubauer, S.C., Troxler, T. and Wigand, C. (2016). Contributions of organic and inorganic matter to sediment volume and accretion in tidal wetlands at steady state. *Earth's Future*, **4**(4), 110–121. ISSN 2328-4277. DOI: 10.1002/2015EF000334.

Morris, M., Hassan, M., Kortenhaus, A. and Visser, P. (2009). Breaching Processes: A state of the art review, Technical Report FLOODsite T06-06-03, HR Wallingford, UK.

Narayan, S., Beck, M.W., Reguero, B.G., Losada, I.J., van Wesenbeeck, B., Pontee, N., Sanchirico, J.N., Ingram, J.C., Lange, G.M. and Burks-Copes, K.A. (2016). The Effectiveness, Costs and Coastal Protection Benefits of Natural and Nature-Based Defences. *PLOS ONE*, **11**(5), e0154735. ISSN 1932-6203. DOI:10.1371/journal.pone.0154735.

Neumann, B., Vafeidis, A.T., Zimmermann, J. and Nicholls, R.J. (2015). Future Coastal Population Growth and Exposure to Sea-Level Rise and Coastal Flooding - A Global Assessment. *PLOS ONE*, **10**(3), e0118571. ISSN 1932-6203. DOI:10.1371/journal.pone.0118571.

Peeters, P., Van Hoestenberghe, T., Vincke, L. and Visser, P.J. (2011). SWOT analysis of breach models for common dike failure mechanisms, In: *Proceedings of the 34th IAHR World Congress (Brisbane, 2011)*, 3936–3943.

Pontee, N. (2013). Defining coastal squeeze: A discussion. *Ocean & Coastal Management*, **84**, 204–207. ISSN 09645691. DOI:10.1016/j.ocecoaman.2013.07.010.

Rijkswaterstaat and KNMI (1961). Verslag over de stormvloed van 1953, Technical report, RWS & KNMI, 's-Gravenhage.

Saintilan, N., Kovalenko, K.E., Guntenspergen, G., Rogers, K., Lynch, J.C., Cahoon, D.R., Lovelock, C.E., Friess, D.A., Ashe, E., Krauss, K.W., Cormier, N., Spencer, T., Adams, J., Raw, J., Ibanez, C., Scarton, F., Temmerman, S., Meire, P., Maris, T., Thorne, K., Brazner, J., Chmura, G.L., Bowron, T., Gamage, V.P., Cressman, K., Endris, C., Marconi, C., Marcum, P., St. Laurent, K., Reay, W., Raposa, K.B., Garwood, J.A. and Khan, N. (2022). Constraints on the adjustment of tidal marshes to accelerating sea level rise. *Science*, **377**(6605), 523–527. ISSN 0036-8075. DOI:10.1126/science.abo7872.

Schoutens, K., Stoorvogel, M., van den Berg, M., van den Hoven, K., Bouma, T.J., Aarninkhof, S., Herman, P.M.J., van Loon-Steensma, J.M., Meire, P., Schoelynck, J., Peeters, P. and Temmerman, S. (2022). Stability of a Tidal Marsh Under Very High Flow Velocities and Implications for Nature-Based Flood Defense. *Frontiers in Marine Science*, **9**. ISSN 2296-7745. DOI:10.3389/fmars.2022.920480.

Scott, D.B., Frail-Gauthier, J. and Mudie, P.J. (2014). *Coastal Wetlands of the World*, Cambridge University Press.

Stoorvogel, M.M., Temmerman, S., Oosterlee, L., Schoutens, K., Maris, T., van de Koppel, J., Meire, P. and Bouma, T.J. (2024). Nature-based shoreline protection in newly formed tidal marshes is controlled by tidal inundation and sedimentation rate. *Limnology and Oceanography*. ISSN 0024-3590. DOI:10.1002/lno.12676.

Stralberg, D., Brennan, M., Callaway, J.C., Wood, J.K., Schile, L.M., Jongsomjit, D., Kelly, M., Parker, V.T. and Crooks, S. (2011). Evaluating Tidal Marsh Sustainability in the Face of Sea-Level Rise: A Hybrid Modeling Approach Applied to San Francisco Bay. *PLoS ONE*, **6**(11), e27388. ISSN 1932-6203. DOI:10.1371/journal.pone.0027388.

Taherkhani, M., Vitousek, S., Barnard, P.L., Frazer, N., Anderson, T.R. and Fletcher, C.H. (2020). Sea-level rise exponentially increases coastal flood frequency. *Scientific Reports*, **10**(1), 6466. ISSN 2045-2322. DOI:10.1038/s41598-020-62188-4.

Tay, C., Lindsey, E.O., Chin, S.T., McCaughey, J.W., Bekaert, D., Nguyen, M., Hua, H., Manipon, G., Karim, M., Horton, B.P., Li, T. and Hill, E.M. (2022). Sea-level rise from land subsidence in major coastal cities. *Nature Sustainability*, **5**(12), 1049–1057. ISSN 2398-9629. DOI:10.1038/s41893-022-00947-z.

Taylor-Burns, R., Lowrie, C., Tehranirad, B., Lowe, J., Erikson, L., Barnard, P.L., Reguero, B.G. and Beck, M.W. (2024). The value of marsh restoration for flood risk reduction in an urban estuary. *Scientific Reports*, **14**(1), 6856. ISSN 2045-2322. DOI:10.1038/s41598-024-57474-4.

Temmerman, S., Meire, P., Bouma, T.J., Herman, P.M.J., Ysebaert, T. and De Vriend, H.J. (2013). Ecosystem-based coastal defence in the face of global change. *Nature*, **504**(7478), 79–83. ISSN 0028-0836. DOI:10.1038/nature12859.

Van den Berg, M., Rikkert, S., Aarninkhof, S. and Labeur, R. (2024). Assessment of in-situ tidal marsh erodibility under high flow velocities. *Frontiers in Environmental Science*, **12**.

van den Hoven, K., van Belzen, J., Kleinhans, M.G., Schot, D.M., Merry, J., van Loon-Steensma, J.M. and Bouma, T.J. (2023). How natural foreshores offer flood protection during dike breaches: An explorative flume study. *Estuarine, Coastal and Shelf Science*, **294**, 108560. ISSN 02727714. DOI:10.1016/j.ecss.2023.108560.

van Rhee, C. (2010). Sediment Entrainment at High Flow Velocity. *Journal of Hydraulic Engineering*, **136**(9), 572–582. ISSN 0733-9429. DOI:10.1061/(ASCE)HY.1943-7900.0000214.

van Wesenbeeck, B.K., de Boer, W., Narayan, S., van der Star, W.R.L. and de Vries, M.B. (2017). Coastal and riverine ecosystems as adaptive flood defenses under a changing climate. *Mitigation and Adaptation Strategies for Global Change*, **22**(7), 1087–1094. ISSN 1381-2386. DOI:10.1007/s11027-016-9714-z.

Visser, P.J. (1998). *Breach growth in sand-dikes*, Ph.D. thesis, Delft University of Technology, Delft.

Visser, P.J. (1999). Breach Erosion in Sand-Dikes, In: *Coastal Engineering 1998*, 3516–3528, American Society of Civil Engineers, Reston, VA.

Vitousek, S., Barnard, P.L., Fletcher, C.H., Frazer, N., Erikson, L. and Storlazzi, C.D. (2017). Doubling of coastal flooding frequency within decades due to sea-level rise. *Scientific Reports*, **7**(1), 1399. ISSN 2045-2322. DOI: 10.1038/s41598-017-01362-7.

Vousdoukas, M.I., Mentaschi, L., Voukouvalas, E., Verlaan, M., Jevrejeva, S., Jackson, L.P. and Feyen, L. (2018). Global probabilistic projections of extreme sea levels show intensification of coastal flood hazard. *Nature Communications*, **9**(1), 2360. ISSN 2041-1723. DOI:10.1038/s41467-018-04692-w.

Vuik, V., Jonkman, S.N., Borsje, B.W. and Suzuki, T. (2016). Nature-based flood protection: The efficiency of vegetated foreshores for reducing wave loads on coastal dikes. *Coastal Engineering*, **116**, 42–56. ISSN 03783839. DOI:10.1016/j.coastaleng.2016.06.001.

Wahl, T.L. (2007). Laboratory investigations of embankment dam erosion and breach processes, Technical Report T032700-0207A, CEA Technologies inc., dam safety interest group.

Zerihun, Y.T. (2020). Free Flow and Discharge Characteristics of Trapezoidal-Shaped Weirs. *Fluids*, **5**(4), 238. ISSN 2311-5521. DOI:10.3390/fluids5040238.

Zhang, C., Mishra, D.R. and Pennings, S.C. (2019). Mapping salt marsh soil properties using imaging spectroscopy. *ISPRS Journal of Photogrammetry and Remote Sensing*, **148**, 221–234. ISSN 09242716. DOI:10.1016/j.isprsjprs.2019.01.006.

Zhang, P.p., Gong, Y.q., Chua, K.V., Dai, J. and Mao, J.q. (2023). Numerical study of submerged bending vegetation under unidirectional flow. *Water Science and Engineering*. ISSN 16742370. DOI:10.1016/j.wse.2023.06.001.

Zhao, G. (2016). *Breach growth in cohesive embankments due to overtopping*, Ph.D. thesis, Delft University of Technology, Delft.

Zhu, Y. (2006). *Breach Growth in Clay-Dikes*, Ph.D. thesis, Delft University of Technology, Delft.

Zhu, Z., Vuik, V., Visser, P.J., Soens, T., van Wesenbeeck, B., van de Koppel, J., Jonkman, S.N., Temmerman, S. and Bouma, T.J. (2020). Historic storms and the hidden value of coastal wetlands for nature-based flood defence. *Nature Sustainability*, **3**(10), 853–862. ISSN 2398-9629. DOI:10.1038/s41893-020-0556-z.

Appendix A: Test setup

A.1 Test basin and model dike

The Flood Proof Holland facility from VPdelta+ consists of five basins used to test mobile barriers and one (the largest) to test dikes (Figure 12). In this study the largest basin was used, located in the northeast corner. In the centre, two water storage basins are situated. A single gravity pipe connects the water storage basins to a basin. A manual valve for each pipe regulates the flow between two basins. There is a cabin for shelter and measurements, two freight containers for material storage, and a temporary depot to store the sediment.The sides of the basin consist of wooden retaining walls on the north and south ends and roughly 1:3 sloped embankments on the west and east ends. The bottom of the basin adjacent to the retaining walls is made of concrete slabs, and in between (the center) made of a thick clay layer. The concrete slabs extend 3 m up the embankment while the rest of the embankment is grass. Machinery can access the basin through a 1:9 sloped, 3 m wide, concrete slab road situated in the northwest corner of the basin. In the northeast corner, a brick wall is located from other research which could not be (re)moved. Behind the brick wall a small pump is installed which can be used to drain the basin. The gravity inlet pipe to fill the basin is located in the southwest corner.

The model dike had inner and outer slopes of roughly 1:2.5 to 1:3.0. The outer (upstream side) slope was 1:2.5. The inner slope (downstream side) was 1:3.0 at first, but changed to 1:2.5 to increase the downstream basin volume and to prolong tests.

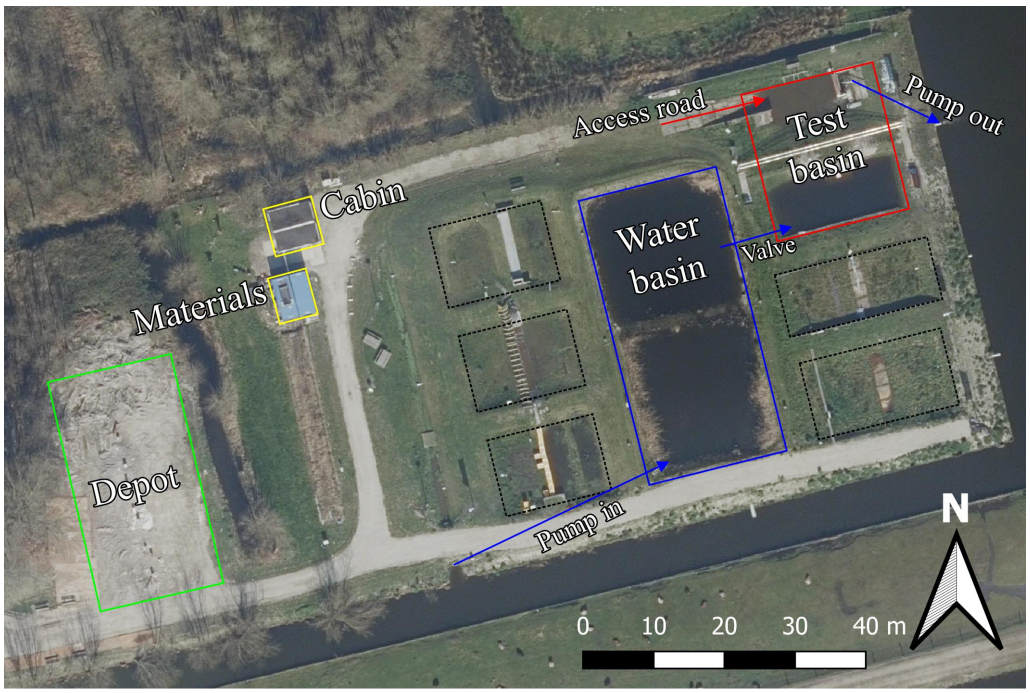

Figure 12: Overview of the Flood Proof Holland facility. The basin used in this study is shown by the red rectangle, and the water storage basin by the blue rectangle. The blue arrows indicate how water is pumped into the water basins, flows to the basin and is pumped out of the basin. The red arrow indicates the access road to the basin floor for machinery. The black rectangles show the other basins of the facility. The depot where all sediment was stored is shown by the green rectangle. The yellow rectangles show the cabin for shelter and measurements (upper) and two freight containers to store materials (lower).

A.2 Pump system

During the planning of the experiment, the expected breach growth rate and associated discharges were estimated using the BRES model by Visser (1998, 1999). The BRES model was developed for overflowing sand dikes and verified with data of the Zwin'94 experiment. In the Zwin'94 experiment North Sea sand was used, similar to the sand used in our experiment (see Table 5). For a 2.0 m high sand-dike using sediment parameters from the Zwin'94 experiment, the model predicted that upstream and downstream water levels would quickly drop/rise due to high discharges relative to the basin storage area, leading to breach development preemptively ending in stage 3. To potentially mitigate

this as much as possible, a pump system was installed at the downstream (north) end of the basin. A total of four submersible pumps were used in parallel with a combined maximum capacity of 1 m^3 s^{-1} (Figure 13A). The pumps were connected to 600 mm diameter steel pipes that ran clockwise to the upstream side (southeast corner) of the basin. Downstream accumulated breach discharge could then be pumped back upstream to mitigate quickly changing water levels. Initially, the exit of the pipe was horizontal, but this resulted in large horizontal flow circulation which eroded the outside slope of the dike. After the first test the end was adjusted to a vertical exit instead (Figure 13B). The spin-up time of the pump system (duration to generate sufficient water head) was recorded to be at least 30 seconds. The pumps were started when the inlets were fully submerged to avoid cavitation, which was around a downstream water level of 50 cm above the basin bottom.

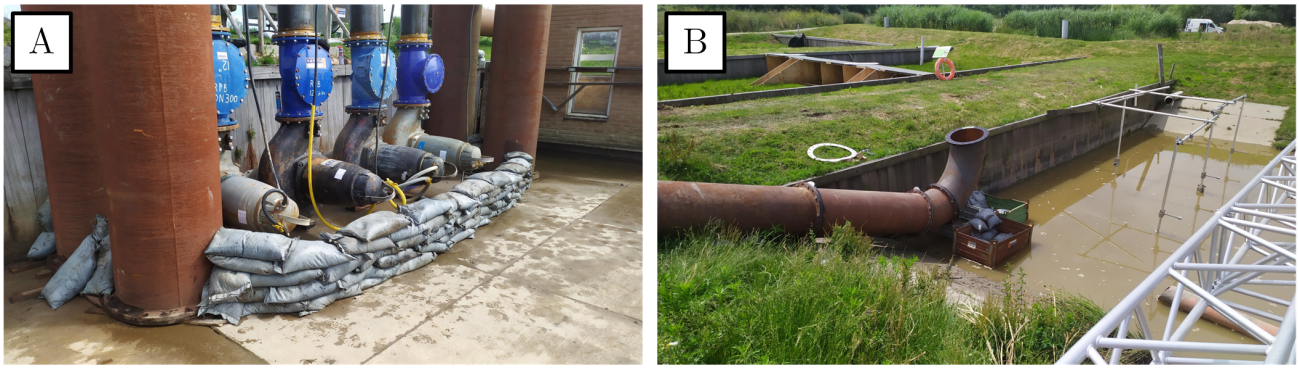

Figure 13: (A) Installed submersible pumps at the north end of the basin. The sandbags prevent clogging of the pump inlets by sedimentation of the eroded sediment. (B) Vertical pipe exit at the southeast corner of the basin to prevent large horizontal circulation in the upstream basin.

A.3 Dike and foreshore sediment characteristics

To determine sand and clay properties, samples were taken in-situ once the dike and foreshore were built. Sand grain size distribution was obtained from a dry sieve analysis. For the clay, first wet sieving was done to separate the sand and fines (<63 μm) fraction. Then, a dry sieve analysis was done on the sand fraction and a hydrometer test (BS 1377-2) on the fine fraction. Permeability of the sand was determined from a constant head test (ASTM-D2434). Atterberg limits of the clay were determined using a falling cone penetration test (liquid limit) and rolling test (plastic limit) conform ISO/TS 17892-12. Cohesion and friction angle were determined from direct shear tests (BS 1377-7). The results are shown in Table 5.

Overall, the sand characteristics are typical for North Sea sand (Kohsiek, 1984). Most notable variability is in the 90^{th} percentile grain diameter (D_{90}) and permeability (k). A variability in D_{90} is easily explained by the different North Sea source locations where the sand was dredged. The variability in permeability may be explained by the coefficient of uniformity (C_u) and coefficient of curvature (C_c). A more uniformly distributed soil (C_u close to unity) is more permeable due to a lack of smaller grains filling the voids. Similarly, a distribution with a curvature close to unity has a more uniform spread of smaller and larger particles, while C_u <1 indicates more smaller particles and vice versa. Here, the dike sand is less uniform and more distributed towards the smaller particles compared to the foreshore sand, and consequently has a smaller permeability.

Dutch river clay is not the same as tidal marsh soil. Nonetheless, the aim of the clay in this study is to act as a low erodible foreshore, similar to a tidal marsh in practice. Therefore, the aim is not to have identical soil properties as a tidal marsh, but model its erosion behaviour. To this extent, the Dutch river clay characteristics are adequate. The sand fraction is on the higher end of what is common for tidal marshes (10-30%, Marin-Diaz et al. (2022)). A water content of 26% is relatively low for a salt marsh, where upwards of 40-50% is more common (Zhang et al., 2019; Marin-Diaz et al., 2022). Soil strength for clay soils at the measured water content is typically largest (Dafalla, 2013; Malizia and Shakoor, 2018), which makes up for the absence of a root system that would otherwise strengthen the soil in a salt marsh (Lo et al., 2017; De Battisti et al., 2019). Furthermore, the clay can be characterised as a low plasticity (PI=23.5%), soft/firm (CI=0.49) clay, which corresponds well with what was observed when constructing the clay foreshore in the basin.

Table 5: Sediment characteristics of the used North Sea sand and Dutch river clay. For some parameters the mean ± standard deviation is given.

Sediment		Sand dike	Sand foreshore	Sediment		Dutch river clay
Parameter	Unit	Value	Value	Parameter	Unit	Value
Sand fraction	%	94.8 ± 0.19	95.5 ± 0.01	Sand fraction	%	36
Fines fraction	%	5.2 ± 0.19	4.5 ± 0.01	Fines fraction	%	64
D_{10}	mm	0.181 ± 0.005	0.171 ± 0.001	Water Content (WC)	%	25.99 ± 1.77
D_{50}	mm	0.243 ± 0.023	0.224 ± 0.003	Liquid Limit (LL)	%	37.40
D_{90}	mm	0.715 ± 0.003	0.440 ± 0.015	Plastic Limit (PL)	%	13.87
Uniformity (C_u)	-	1.82 ± 0.07	1.34 ± 0.02	Plasticity Index (PI)	%	23.53
Curvature (C_c)	-	0.85 ± 0.04	1.04 ± 0.04	Consistency Index (CI)	-	0.49
Porosity (n)	-	0.38	0.41	Cohesion (c)	kPa	27.7
Permeability (k)	m s^{-1}	$3.00 \cdot 10^{-4}$	$3.74 \cdot 10^{-4}$	Friction angle (ϕ)	deg	13.0

Appendix B: Data post-processing

The upstream pressure sensors initially had a 2 Hz measurement frequency, but this was increased to 10 Hz due to wave interference in the basin once the pump system was operational. The downstream sensors and barometer had a 1 Hz burst frequency, averaging 10 measurements and thus had a 0.1 Hz measurement frequency. For post-processing, the first step was to average the upstream measurements to match the downstream 0.1 Hz frequency. Then, the resulting pressures were corrected for atmospheric pressure and their location with respect to the basin bottom to compute the water levels. Missing data due to emerged sensors were estimated from camera footage or linear interpolation (see Figure 14).

The breach width was first obtained from the camera footage facing the front of the breach, from the pixel distance at equal intervals to the pressure sensors (0.1 Hz). The pixel distance was then converted to meters using the 1x1m grid as a reference. Inaccuracies (order 10 cm) in pixel distance measurements was corrected by ensuring a monotonically increasing breach width.

The 3D laser scanner produces pointclouds. Using CloudCompare V2.12.4, the three pointclouds before and after each test were aligned using three reference markers that were placed inside and around the basin. Then, the pointclouds were merged and spliced to only retain the basin area. Lastly, the resulting pointcloud was subsampled with a minimum point distance of 1.5 mm to reduce file size and improve workability. From the scans before a test, the (upstream and downstream) basin volumes were obtained. By overlaying the scans after a test, the eroded sediment volume could be computed. From the measured basin volumes at different heights (step size=0.1 m), the basin storage area A as function of the water level ($A(h)$) was computed (Figure 15). Breach profiles were taken every 0.25 m along the dike axis and cross-sections taken every 0.50 m across the dike axis.

Breach discharge was obtained from the function $Q_{breach} = Q_{\text{in}} - Q_{\text{out}}$. Here, $Q_{\text{in}} = Q_{\text{inflow}} + Q_{\text{pump}}$ and $Q_{\text{out}} = A(h_u) \cdot \Delta h_u$, where $A(h_u)$ is the upstream basin storage area at upstream water level h_u and Δh_u the upstream water level difference over each time interval. Similarly, the inflow discharge Q_{inflow} from the gravity pipe was computed from filling the basin. To measure the pump system discharge Q_{pump}, an electromagnetic flowmeter was used with a 2 Hz measurement frequency. Computer logging was not possible, so a fifth camera (GoPro Hero10, 1080p@60fps) was used to record the sensor display. The data was filtered using a centered moving average with a window length of 20 data points, then linearly interpolated to match pressure sensor frequency (0.1 Hz).

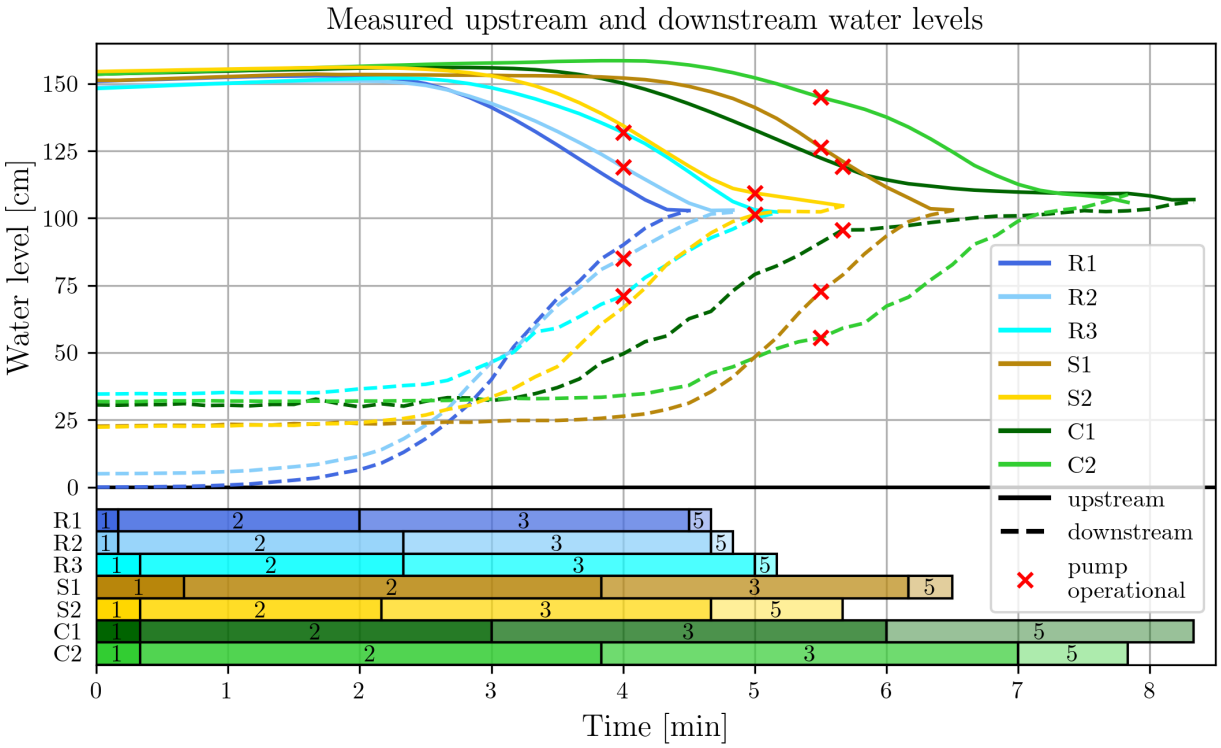

Figure 14: Measured upstream and downstream water levels for each test. The horizontal bar chart shows the breach stage as recorded (Table 2). Note: During tests R1, R2 and S2 the pressure sensors were emerged for part of the test duration. Missing data was simulated. For tests R1 and R2 the downstream water level from 0-3 minutes was simulated from video footage, and for test S2 the upstream water level was linearly interpolated after 5:00 minutes.

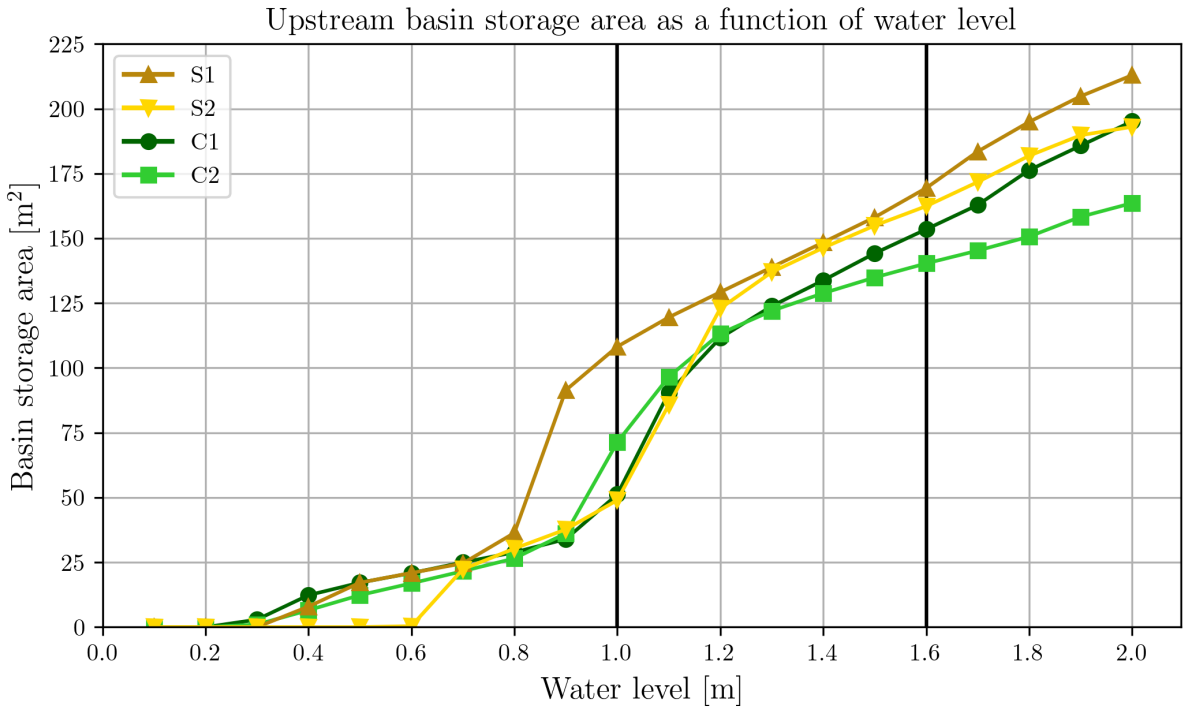

Figure 15: Measured upstream basin storage area as a function of water level at 0.1 m increments. Storage area was computed from the volume change each increment. For the reference tests the values for test S1 were used. The vertical black lines indicate the effective range used to compute the discharges from the upstream basin water level change rate.

Appendix C: Test procedure

After the construction of the dike (and foreshore), test execution took the entire next day (about 8 hours). The morning routine consisted of preparing, programming and installing the pressure sensors. The sensors were set to start recording at a specified time early in the afternoon. Then, the 1x1 m grid was spray painted on the inner dike slope, followed by the 3D scans (only for the foreshore tests). When the set time for the pressure had passed, the upstream basin was filled. Meanwhile, the cameras were installed and connected to a remote control for synchronisation. No waterproof cover to reduce the phreatic line was placed on the upstream slope of the dike. Although such a cover would prevent macro instability of the dike slopes, it could negatively impact the breaching process. Instead, to limit the probability of macro instability, the test was started soon after the basin was filled. When the desired upstream water level (≈1.5 m or above) was reached, the cameras were started and an incision (20-40 cm wide) in the dike crest was dug with a shovel. Inflow to the basin Q_{inflow} continued throughout a test unless the level was close to exceeding dike height. Once flow on the inner slope was established and reached the inner toe of the dike this time was recorded as t_0. During the test, the small excavator continuously removed some of the sediment directly deposited at the breach exit. This was done to compensate for the fast rising downstream water level which greatly reduced outflow velocities at the breach exit leading to increased sedimentation. Nonetheless, removal of the sediment appeared to have a marginal effect. The pumps were started once their inlets were fully submerged. Once upstream and downstream water levels equalled (equilibrium water level) the test ended, which sometimes coincided with stopping the pump system. Then, the cameras were stopped and the basin was drained. When the basin was empty, more 3D scans were done (only for foreshores tests) and the sensors were removed, stopped and the data extracted. The next days the eroded dike (and foreshore) sediment was removed from the basin. The remaining sediment in the breach was slurry (like quicksand) and was therefore also removed. New sediment was added and mixed with the remaining dike material to construct the new dike. The foreshore was locally removed to construct the new dike and afterwards mixed with new foreshore sediment to reconstruct it. When completed, a new test could be done. The first dike took roughly 4 days to construct. For the other tests construction, test and repair would take 3 days. An extra day was necessary to construct the first sandy foreshore and switch to the clay foreshore.

Appendix D: Details of general breach development

During stage 1 a staircase profile developed. The process that led to this is as follows: first, sediment pick-up by the flow along the slope increases the sediment concentration, and simultaneously increases the slope angle (steepness). At some point along the slope, before reaching the toe of the slope, the sediment concentration in the flow is maximum, reaching sediment transport capacity (STC). Once STC is achieved, sediment pick-up (erosion) and deposition (sedimentation) rates are equal. Downstream of this location the original slope angle is retained. Consequently, as upstream the slope angle continuously increases, the flow encounters a step and a pool is formed where sedimentation occurs (lowering sediment concentration). The pool overflow can then again pick-up sediment along the slope and another step is created until the flow reaches the toe of the slope. Throughout stage 1 the number of steps decreased as on average the slope steepened, and remained mostly constant in stage 2. The cause may be insufficient STC (staircase profile) to visually steepen the slope. This is supported by the observation that in stage 3 the number of steps decreased to none and steeper water surface profiles were observed.